2019-03-01

# Wasatch Front Atmospheric Deposition Reflects Regional Desert Dust and Local Anthropogenic Sources

Michael Max Goodman
*Brigham Young University*

# Wasatch Front Atmospheric Deposition Reflects Regional Desert Dust and Local Anthropogenic Sources

Michael Max Goodman

A thesis submitted to the faculty of
Brigham Young University
in partial fulfillment of the requirements for the degree of

Master of Science

Gregory T. Carling, Chair
Stephen T. Nelson
Barry R. Bickmore

Department of Geological Sciences

Brigham Young University

ABSTRACT

Wasatch Front Atmospheric Deposition Reflects Regional Desert Dust and Local Anthropogenic Sources

Michael Max Goodman
Department of Geological Sciences, BYU
Master of Science

Dust originating from dry lakes contributes harmful and toxic elements to downwind urban areas and mountain snowpack that is compounded by local contaminant inputs from anthropogenic sources. To evaluate dust contributions to an urban area from regional playas, we sampled playa dust sources, urban dust deposition, and snow dust deposition in central Utah, USA. Samples were analyzed for grain size, mineralogy, and chemistry. Bulk mineralogy between playa, urban, and snow dust samples was similar, with silicate, carbonate, and evaporite minerals. Grain size distribution between fine playa, urban, and snow dust particles was also similar. Elements found at high concentrations in playas include Li, Na, Mg, Ca, Sr, and U, and most other elements were found at higher concentrations in urban and snow deposition samples. Particularly enriched elements in dust deposition include Cu, Se, Ag, Cd, Sb, and La, which are sourced from industrial activity, mining, and vehicular emissions and wear. Based on results from mass balance modeling, a large majority of the dust mass deposited on the Wasatch Front is from playa sources. Urban and playa dust sources largely remain constant seasonally, although spikes in playa-associated element concentrations during a particular seasonal sample may indicate frequent and/or more intense dust events. Among the highly environmentally available elements B, Ca, Sr, and U, are Cd and Se, both of which present toxicity concerns for humans and environments. This is the first study describing heavy metal contamination and sources in Utah, USA.

Key Words: playa dust, mineral dust, urban dust, dust chemistry

ACKNOWLEDGMENTS

I would like to specifically thank the help of my advisor Dr. Greg Carling for his support through each step of my thesis. I would also like to thank Dr. Barry Bickmore and Dr. Steve Nelson for their assistance and recommendations. For help with various lab methods I would like to thank Dr. Diego Fernandez at the University of Utah and Dr. Jeff Munroe at Middebury College. A special thanks goes out to Kevin Rey and fellow students Andrew Bentz and Trent Taylor for assisting with field and lab work. Thank you to Jennifer DeGraffenried and Christopher Bradbury for taking us to the Dugway Proving Grounds and allowing us to place a BSNE on site. Above all, I am thankful for my wife, Kristin, who took care of me and the kids while I put in long hours to create this thesis.

TABLE OF CONTENTS

LIST OF TABLES

LIST OF FIGURES

# 1. Introduction

Saline lakes across the globe are quickly drying because of climate change and water diversions (Wurtsbaugh et al., 2017). This change is exposing large areas of dry lakebed and playas that are significant sources of mineral dust (Prospero et al., 2002; Reynolds et al., 2007; Goudie, 2009; Steenburgh et al., 2012; Wurtsbaugh et al., 2017; Skiles et al., 2018). One example is Owens (dry) Lake at the edge of the Great Basin in California, where increased dust emissions have resulted in $PM_{10}$ (particulate matter <10 μm) exceedances and deposition of harmful metals in downwind communities (Cahill et al., 1996; Gill, 1996; Reheis, 1997; Reheis et al., 2002, 2009). Consistent drought in the 1960s in Africa dried up part of Lake Chad, forming the Bodélé Depression, which is the world's premier dust source (Washington et al., 2003). In the western US, dust deposition has increased 500% in the last century, highlighting the need and urgency to understand its mineral, chemical, and biological makeup (Neff et al., 2008). Mineral dust emitted from dry lakes has a variety of adverse effects to the environment and human health. For example, dust carries a variety of organisms, metals, and nutrients that can contaminate water resources (Kellogg and Griffin, 2006; McTainsh and Strong, 2007; Carling et al., 2012; Dastrup et al., 2018), may cause diseases such as asthma, pneumonia, and valley fever in humans (Pope et al., 1991; Derbyshire, 2007; Goudie, 2014), can increase the frequency and intensity of harmful algal blooms, especially in remote areas (Zhang, 1994; Brahney et al., 2015), and can cause earlier snowmelt and decreased runoff in mountain snowpack (Painter et al., 2010, 2010).

Mineral dust mixed with urban aerosols determines the composition of dust particles. The bulk composition of mineral dust includes silicate, carbonate, and evaporite minerals, with high concentrations of crustal elements such as Al, Ca, Fe, K, Mg, Na, and Si (Kubilay and Saydam,

1995; Reheis et al., 2009; Abed et al., 2009). Variation in dust chemistry is largely found in trace element concentrations (Ben-Israel et al., 2015; Zhao et al., 2015), such as the enrichment of Se in dust from the Salton Sea lakebed in California (Williams, 1935; Frie et al., 2017). Furthermore, toxic and trace elements are enriched in $PM_{2.5}$ fractions relative to larger size fractions (Das et al., 2015; Aarons et al., 2017). In urban settings, anthropogenic sources of particulate matter include, but is not limited to, refining, combustion, vehicle exhaust, tire and brake abrasion, construction, gravel pits, and mining (Ajmone-Marsan and Biasioli, 2010; Gunawardana et al., 2012). These urban aerosols mix with mineral dust to create a dust mixture (hereafter labeled "urban dust") that is enriched in trace and heavy metals (Lee et al., 1972; Li et al., 2001; Divrikli et al., 2003; Samara and Voutsa, 2005; Das et al., 2015). Sequential leaching of dust samples can be used to estimate the partitioning of elements among different compositional fractions, which has implications for element availability or immobility (Lawrence et al., 2010; Carling et al., 2012; Dastrup et al., 2018).

To interpret dust chemistry differences, a variety of sampling methods, analyses, and statistical methods are commonly required. For example, dust deposition flux rates are estimated using dust collectors with a known surface area that are deployed for a fixed period of time (Wake et al., 1994; Reheis and Kihl, 1995; Reheis, 1997; Liu et al., 2011). Relative abundances of elements in particular dust samples are interpreted with enrichment diagrams (Reimann and de Caritat, 2005). Enrichment diagrams are created by normalizing element concentrations to background concentrations and then plotting the relative enrichment or depletion. Principal components analysis (PCA) is a technique used to distinguish individual dust samples by performing an orthogonal transformation which converts a set of observations of somewhat correlated variables into principal components (PCs). When evaluating urban atmospheric

contamination, different PCs are used to characterize specific urban aerosol sources based the elements principally described by each PC (Tokalıoğlu and Kartal, 2006; Meza-Figueroa et al., 2007; Gunawardana et al., 2012).

The purpose of this study is to determine the source of dust deposition along the Wasatch Front in Utah. Specific objectives include to: 1) compare dust chemistry and mineralogy of major playa dust sources to urban and snow dust deposition; 2) estimate urban aerosol and playa dust contributions to total Wasatch Front dust deposition; 3) evaluate seasonal variability in urban dust deposition fluxes and chemistry; and 4) characterize the environmental availability of toxic elements in urban and snow dust deposition.

In northern Utah, more than two million people live along the north-south trending Wasatch Front, which marks the eastern edge of the Basin and Range province (Fig. 1). The Wasatch Front experiences regular dust storms due to proximity to regional dust sources (Jewell and Nicoll, 2011; Steenburgh et al., 2012; Hahnenberger and Nicoll, 2012; Reynolds et al., 2014; Mallia et al., 2017). HYSPLIT backward trajectories, satellite images, and models have shown that Great Basin playas are significant dust sources downwind of the Wasatch Front (Hahnenberger and Nicoll, 2014; Skiles et al., 2018; Dastrup et al., 2018) Mineral dust sources include playas in the Sevier Desert and Great Salt Lake Desert (Fig. 1). The Great Salt Lake, a hypersaline terminal lake, is an increasingly important dust source that continues to dry because of drought and river diversion, increasing the lakebed surface area available for dust mobilization (Wurtsbaugh et al., 2017). The urban aerosol sources along the Wasatch Front include oil and gas combustion, vehicle exhaust, tire and brake abrasion, gravel pits, construction, mining, refining, and various types of industry emissions. Mineral dust from playas mixes with these

urban aerosols to create urban dust deposition along the Wasatch Front and in nearby mountain snowpack.

## 2. Study Area

Basins of the Sevier Desert and Great Salt Lake Desert were once part of the Pleistocene Lake Bonneville, the remnant of which is the Great Salt Lake and several playas (Fig. 1) (Hahnenberger and Nicoll, 2012; Steenburgh et al., 2012; Reynolds et al., 2014). Due to flooding events, Lake Bonneville drained and separated 10,070 ± 130 14C years before present into north and south arms, creating different hydrogeological systems (Oviatt, 1988; Hart, 2004). The north arm has slowly dried up, leaving behind the Great Salt Lake Desert and Tule Valley playas. The remaining body of water is the Great Salt Lake, which in July 2016 experienced an elevation drop to a historic low elevation, exposing more than 50% of the lakebed. The south arm of Lake Bonneville, Lake Gunnison, has continued to dry for the last 10,000 years, leaving behind multiple dry lakebeds including Sevier Dry Lake and the Wah Wah playa. Sevier Dry Lake remained filled with water until the mid-1800's, when it transitioned into a playa due to irrigation diversions. It has remained dry until the present, with the exception of a high snow-melt runoff period from 1984-1985, briefly flooding the lakebed with water (Oviatt, 1988) Currently, Sevier Dry Lake and the Great Salt Lake lakebed have similar surface conditions, with rigid, crusty sediment on top and wet, clay-rich sediments underneath.

In Utah, meteorological conditions produce dust storms on a seasonal basis. Dust storms typically occur during the spring and fall seasons (Steenburgh et al., 2012; Hahnenberger and Nicoll, 2012). There are an average of 4.3-4.7 dust events per year, and many are associated with a cold front or a baroclinic trough producing southwesterly winds above threshold friction velocities to entrain sediments (Jewell and Nicoll, 2011; Steenburgh et al., 2012; Hahnenberger

and Nicoll, 2012). These southwesterly winds funnel through the Basin and Range topography towards the urban Wasatch Mountains, entraining playa sediments along the way (Hahnenberger and Nicoll, 2012).

## 3. Sampling and Methods

### *3.1 Playa Dust Source Sampling*

To sample representative playa dust sources, a total of 14 separate locations were selected including Sevier Dry Lake (SDL), Tule Valley (TV), Wah Wah Valley (WW), Sunstone Knoll (SK), Fumarole Butte (FB), Pismire Wash (PW), Fish Springs (FS), Dugway Proving Grounds (DPG), and the dry lakebed of Great Salt Lake (GSL) (Fig. 1). BSNE (Big Springs Number Eight) samplers, which are traps installed at a fixed height above the ground and directed into the wind by a fin (Fryrear, 1986), were deployed at each location. Two types of BSNE samplers were used; the four-port sampler has four traps at heights of approximately 10 cm, 15 cm, 20 cm and 40 cm, and the single-port sampler has one trap at approximately 40cm. For the first sampling period, all samplers except the DPG sampler were deployed in February and March 2016 and collected in May 2016 and again in September or October 2016. The FB sample was collected three times during the sampling window because the traps rapidly filled with dust. In September and October 2016, all samplers were removed except those at GSL sites, and the GSL4 single sampler was replaced with a four-port sampler (Fig. 1). The third and final collection of GSL samples was during October 2016 through June 2017. The GSL1 sampler from this collection period was knocked over and no sample was recovered. A four-port sampler was deployed at DPG in April 2017 and collected in October 2017.

Dust collected from each of the four ports was collected and analyzed as a separate sample (Fig. 1). Samples were collected by removing the trap, adding ultra-pure water, and pouring the dust slurry into bags, repeating as necessary to ensure complete sample collection.

Because many playa dust source samples had visibly large grains that would not travel regional distances, some dust source samples were wet sieved (hereafter named "fine playa samples"). All dust source samples from the second and third collection periods (Feb/March-Sep/Oct 2016 and Sep/Oct-June 2016-7) were sieved through a 52 μm nylon mesh filter screen in preparation for analysis. For direct comparison between fine and bulk playa dust samples, 7 individual samples were prepared for analyses on both the fine and bulk fractions. In total, 78 unique dust source samples were analyzed for trace and major element chemistry, including 37 bulk and 41 fine.

*3.2 Urban Dust Deposition Sampling*

To characterize dust deposition along the Wasatch Front, dust samples were collected at Brigham Young University in Provo (Provo), University of Utah in Salt Lake City (SLC), Weber State University in Ogden (Ogden), and Utah State University in Logan (Logan). At each city location, we deployed a passive dust collector that is constructed from a 50 gallon tote lined with a plastic bag and covered with an acid-leached plastic screen and marbles to provide a surface for dust deposition (Reheis and Kihl, 1995). To minimize local disturbance, the collectors were placed on the rooftops of university buildings. Samples from each of these locations were collected for the September to November 2015 period and February to May 2016 period, representing both fall and spring dust deposition. The Feb-May 2016 Ogden sample was lost because of sampler malfunction during a high-wind event. During each of those periods, a second collector was placed at the Provo location for eight and 18 days in fall 2015 and spring

2016, respectively, when weather forecasts predicted strong cold fronts and associated dust events. All four samplers were again deployed in June 2017 and samples were gathered in August 2017, October 2017, January 2018, March 2018, May 2018, July 2018, and September 2018, providing a total of 9 urban dust deposition sampling seasons. The Provo and SLC samples collected in August 2018 were lost during sample preparation. In total, 35 urban dust samples were collected: 10 from Provo, 8 from SLC, 8 from Ogden, and 9 from Logan. For each urban dust sample, a deposition flux rate in $g/m^2$/month was calculated based on the area of the bucket, the mass of dust collected, and the number of days that the sampler was left for collection.

*3.3 Snow Dust Deposition Sampling*

To compare dust chemistry in the urban area with dust in adjacent mountains, dust deposition was sampled from mountain snowpack in the Wasatch and Uinta Mountains during spring 2016, 2017, and 2018. To collect dust from these locations, we dug pits in the snow pack, identified dust layers in the snow, and packed 2L FLPE bottles full of sample. In 2016, U1 and W5 were sampled; in 2017, W1, W3, W5, and U2 were sampled; in 2018, W2, W3, W4, W5, W6, W7, U1, U2, and U3 were sampled (Fig. 1). Some locations produced more than 1 sample per season due to multiple dust layers within the snowpack, each of which represents a single dust event or storm. In total, 23 snow dust samples were collected: three in 2016, six in 2017, and 14 in 2018.

*3.4 Sample Analyses*

Dust samples were analyzed for trace and major element concentrations, mineral content, and grain size distribution. In preparation, the dust and water slurries from all 136 source, urban, and snow samples were transferred into acid-washed 2 liter FLPE bottles. Samples were dried by

evaporating at <60°C in a laminar flow hood. To remove organic material, 4 mL 30% hydrogen peroxide was added to the samples. The remaining sample was dried in a laminar flow hood and then crushed for analyses.

Dust samples were analyzed for trace and major element concentrations following a four-step sequential leaching procedure. The total concentration of each element was calculated as the sum of the four leach steps. About 200 mg of dust from each sample was separated (actual amounts ranged from 3 to 350 mg). To each sample, we added 4 mL of a pH = 7 buffer of 1M ammonium acetate ($NH_4AcO$) and the sample was stirred vigorously. Samples were left to equilibrate for ~20 hours, followed by centrifugation at 5000 rpm for 3-5 minutes. The sample was then rinsed with an additional 1 mL of the pH = 7 buffer, stirred, centrifuged, and poured and pipetted into the same new tube. These procedures were repeated on the same dust samples with 1 molar acetic acid ($CH_3COOH$) and 1 molar nitric acid ($HNO_3$). Then, 1 mL of aqua regia (1 part nitric acid mixed with 3 parts hydrochloric acid) was added to the remaining dust sample, which was then diluted to ~10 mL with ultra-pure water. The ammonium acetate leach represents the exchangeable and water-soluble fractions, the acetic acid leach represents the carbonate mineral fraction, the nitric acid leach represents the feldspar and clay fractions, and the acetic acid leach represents the residual fraction, although not all silicate and refractory minerals were completely dissolved (Lawrence and Neff, 2009; Carling et al., 2012; Dastrup et al., 2018).

Each of the four leachates were analyzed for trace element and major element concentrations using an Agilent 7500ce quadrupole inductively coupled plasma mass spectrometer (ICP-MS) with a collision cell, a double-pass spray chamber with perfluoroalkoxy (PFA) nebulizer (0.1 mL/min), a quartz torch, and platinum cones. Concentrations were measured for the following 46 elements: Ag, Al, As, B, Ba, Be, Ca, Cd, Ce, Co, Cr, Cs, Cu, Dy,

Er, Eu, Fe, Gd, Ho, K, La, Li, Lu, Mg, Mn, Mo, Na, Nd, Ni, Pb, Pr, Rb, Sb, Sc, Se, Sm, Sr, Tb, Th, Ti, Tl, U, V, Y, Yb, and Zn. The detection limit (DL) was determined as three times the standard deviation of all blanks analyzed throughout each run. A USGS standard reference sample (T-205) and NIST standard reference material (SRM 1643e) were analyzed multiple times in each run together with the samples as a continuing calibration verification. The long-term reproducibility for T-205 and SRM 1643e show that our results are accurate within 10% for most elements.

Dust mineralogy was evaluated on a subset of six bulk playa, fine playa, and dust deposition samples (18 in all) with x-ray diffraction (XRD). Samples were analyzed on zero background holders with a Rigaku MiniFlex 600 XRD. Resulting patterns were quantitatively interpreted the Reference Intensity Ratio (RIR) method with the Rigaku PDXL2 software. For the RIR method, weight ratios are calculated from given intensity ratios of the substance normalized to a known standard and its highest peak intensity (Hubbard et al., 1976).

A subset of ten bulk playa, fine playa, urban, and snow samples (40 in all) were analyzed for particle size distribution. Each sample was dispersed using sodium hexametaphosphate and then sonified to effectively separate aggregates. Grain-size distribution was measured by laser scattering with a Horiba LA-950 (Munroe et al., 2015), which has an effective range of 50 nm to 3 mm.

*3.5 Data Quality Control*

To prepare the dataset for statistical analyses, we removed some elements or samples that were outliers. For instance, Sc was removed because it was below DL in the majority of samples in all leach steps. For other elements, specific values <DL were set as ½ the DL. Additionally, Pb and Zn were not considered when evaluating playa chemistry because of anomalously high

concentrations that were related to probable contamination from the metal and/or paint on the BSNE samplers (Reynolds et al., 2014). Additionally, several samples were entirely removed from further consideration due to sample preparation errors (two playa dust samples), elevated Cu and Mn concentrations (two GSL playa dust samples), and insufficient samples mass (one snow dust sample).

### *3.6 Data Analysis*

Raw chemistry data was interpreted with enrichment diagrams. Concentrations of all elements from all fine playa samples (n = 39) were averaged to obtain a background chemical signature. Average snow (n = 22), Provo (n = 10), SLC (n = 8), Ogden (n = 8), and Logan (n = 9) samples were divided by the background chemical signature to obtain relative enrichment or depletion for each element.

Similarities and differences in element concentrations between dust types were evaluated with PCA. The software Matlab was used to conduct PCA, producing new axes, or principal components (PC) which explain a fraction of the variance determined by all element concentrations. Each element was assigned a score for each PC, and elements with higher scores principally explain the variance described by the defined PC. PCA scores were interpreted to geochemically distinguish dust samples. Two PCA ordinations were run, one comparing fine and bulk playa dust source chemistry (n= 76) and another comparing fine dust sources (n = 39) with urban (n=35) and snow dust (n=22) deposition chemistry. Each run used total concentrations from the four sequential extraction steps of all elements.

## 4. Results

### *4.1 Similar Chemistry of Playa Dust Sources*

The PCA results showed that both bulk and fine playa dust source samples contained similar trace and major element composition (Fig. 2). A two-axis PCA explained 65.7% of the variance in the dataset (50.5% in PC1 and 15.2% in PC2). PC1 was primarily explained by Be, Al, Mn, Fe, Co, Y, REE's, and Th, while PC2 was explained by Li, B, As, Se, Rb, Sr, Cd, Cs, and U. Samples from the different playas had overlapped in PCA space. Seven samples had both the fine and bulk fraction analyzed, and their similar PC1 and PC2 scores indicate similar chemistry between the size fractions. Given the similar chemistry of the bulk and fine playa samples, only the fine playa samples are considered to simplify the comparisons between playa source and fine-grained urban and snow deposition.

Although bulk geochemistry is similar in the different playas, there were some chemical differences. The playas FB, WW, and PW had relatively higher PC1 scores and corresponding element concentrations, and TV, SK, and GSL have relatively higher PC2 scores and corresponding element concentrations. All eight samples from TV2 are the most unique among all other playa samples, with high PC2 scores and the highest concentrations of As, Sr, Mo, Cs, and U. Relative to other playas, Mo is enriched by two orders of magnitude, and As, Sr, Cs, and U are enriched by a factor of 2-10. Other playas exhibit no significant trends of enrichment or depletion.

*4.2 Mineralogy and Grain Size Similarities Among Fine Playa, Urban, and Snow Dust Samples*

The playa, urban, and snow dust samples contained a similar suite of minerals at different relative abundances (Fig. 3). All samples were comprised of a mix of quartz, halite, gypsum, calcite, aragonite, dolomite, and feldspars (undifferentiated). The GSL sample had >37% aragonite, whereas all other playa samples had very little aragonite. TV and FB had >45% calcite, SDL had >50% halite, and DPG had >50% quartz. Minimal amounts of gypsum (<5%)

was observed in all fine playa samples. The snow dust sample U2 was composed of 52% feldspar and 38% quartz with <1% halite and gypsum. Urban dusts had 20-65% quartz and a mix of halite, gypsum, calcite, aragonite, dolomite, and feldspar. The only urban sample with significant amounts (>1%) of aragonite was Logan with 34%.

Grain sizes were similar between fine playa, snow, and urban dust samples (Fig. 4). All samples are primarily very fine sand to very fine silt, or 125 μm or smaller. The highest concentration of particles is very fine silt (3.91-7.81 μm) among fine playa samples, and medium silt (15.63-31.25 μm) among urban and snow samples. In comparison with the fine playa fraction, urban and snow dusts have a larger fraction of medium silt, coarse silt, and very fine sand fractions, although the differences are negligible within standard deviation error bars.

*4.3 Urban and Snow Enrichment of Trace Metals Relative to Playas*

Fine playa dust was geochemically distinct from snow and urban dust based off of the PCA analysis (Fig. 5). PC1 is primarily explained Be, Al, V, Mn, Fe, Co, Y, REE's, and Th, PC2 is primarily explained by B, Mg, Ca, As, Se, Rb, Sr, Cs, and U, and PC3 is characteristic of Se, Cd, and Sb. Urban and snow dust samples generally have higher PC1 scores and are enriched in corresponding elements. PC2 scores are similar between all dust types, although minor enrichment in fine playa samples is observed. PC3 scores are substantially enriched in urban samples and mostly similar between snow and fine playa samples.

Specific elements vary in concentration between dust types. Averages and standard deviations of the total concentration of each element for fine playa, snow, Provo, SLC, Ogden, and Logan dust types are reported (Table 1). The enrichment diagram (Fig. 6) comparing dust each dust deposition type with the average fine playa sample highlights differences in specific element concentrations. Peaks in enrichment factor values represent higher concentrations, or

enrichment, in dust deposition samples relative to fine playa samples, and troughs represent lower concentrations, or depletion, in dust deposition samples. Box plots showing the actual concentration differences of the depleted elements Li, Na, Mg, Ca, Sr, and U in deposition samples relative to fine playa samples were created (Fig. 7). Box plots were also created for the most enriched elements Cu, Se, Ag, Cd, Sb, and La in deposition samples relative to fine playa samples (Fig. 8).

*4.4 Dust Deposition Flux Rates and Chemistry*

Urban dust deposition flux rates vary by collection season and location. Monthly dust fluxes for each urban dust deposition location varied from 0.5 to 3.9 $g/m^2$/month (Table 2). Seasonally, the highest flux rates were observed in Mar-May 2018 samples with an average of 2.9 $g/m^2$/month, and the lowest were observed in Sep-Nov 2015 samples with an average of 1.0 $g/m^2$/month. Average flux rates of all samples for each location are 2.0, 2.6, 2.4, and 1.8 $g/m^2$/month for Provo, SLC, Ogden, and Logan, respectively. The annual flux rates were 28.7, 34.9, 33.76, and 24.75 $g/m^2$/yr for Provo, SLC, Ogden, and Logan, respectively.

Urban deposition samples showed seasonal similarities and differences in dust chemistry across locations. No seasonal trends were observed for the majority of elements. However, there was a spike in Sr and Na concentrations and a dip in Co and Se concentrations at all four urban locations during the Jan-Mar 2018 sample period (Fig. 9).

*4.5 Sequential Leach Step Comparisons*

To evaluate relative environmental availability of specific elements, element concentrations were compared between each leach step (Fig. 10). All elements from each leach step for fine playa (n = 39), snow (n = 22), and urban deposition (n = 35) samples were averaged

separately to view differences. Based on all elements combined, playa samples have the highest amount of element mass in the ammonium acetate and acetic acid fractions, followed by urban and then snow dust samples. Sodium is the most soluble element in all sampling types, followed by Ca, Sr, Se, U, B, and Cd, all of which had >50% dissolved in the first two leach steps in each sample type. Elements primarily extracted with aqua regia include Cr, Cs, Fe, and Ti in all sample types. The trends for each element remain relatively consistent between all sample types, with large exceptions found largely in the ammonium acetate leach. Zinc and Pb were removed from the fine playa subset due to suspected contamination by the BSNE samplers.

## 5. Discussion

### *5.1 Wasatch Front Dust Deposition Is a Mixture of Playa Dust and Urban Aerosols*

Grain size similarities between playa dust and urban and snow dust deposition confirm that Utah playas are a major source of Wasatch Front atmospheric deposition. In many parts of the world, however, modern global dust sources such as those in Africa and Asia can be the primary mineral and nutrient dust sources (Takemura et al., 2002; Bartholet, 2012). However, Asian aerosols in North America are generally within the <2.5 μm size range (VanCuren and Cahill, 2002; Fairlie et al., 2007), and African dust in western North America generally consists of <1μm particles at low concentrations (Perry et al., 1997). In our study, urban and snow dust deposition particle sizes were in a similar size range as fine playa samples, ranging from 2 μm to 125 μm. The <2μm fraction makes up <4% of the urban and snow sample grains (Fig. 4), indicating that global dust sources are not significantly contributing to the total dust deposition along the Wasatch Front. In our study, grain size indicates that regional playas source the majority of dust to urban and snow deposition.

The mineral composition of regional playa dust sources explains the urban and snow dust deposition mineralogy. Because the mineral suite is the same between playa dust sources and urban and snow dust deposition (Fig. 3), we infer that playas are sourcing the bulk of the mass deposited on the Wasatch Front. Additionally, this same suite of minerals has been described as common dust mineralogy in Utah snowpack (Munroe et al., 2015; Dastrup et al., 2018). However, some minerals such as halite and gypsum may not be effectively transported regional distances due to their high solubility. In the presence of low pH water, calcite and aragonite can (to a much lesser extent) dissolve during transport and deposition along the Wasatch Front. The rather insoluble minerals such as feldspars and silicates are most effectively transported regional distances and are expected to be found at higher percentages in dust deposition. In support of this idea, principal components comparing fine playa with urban and snow dust samples (Fig. 5) are primarily explained by elements found in different mineral suites. Specifically, PC1 can be explained by evaporite and carbonate minerals, and PC2 can be explained by silicate minerals. Generally, playas are more enriched in PC1 and snow and urban samples are more enriched in PC2, confirming that silicate minerals are transported more effectively that evaporite and carbonate minerals from playas to the Wasatch Front.

Dust chemistry data indicates that dust deposition along the Wasatch Front is a mixture of playa dust and urban anthropogenic contamination. In fine playa samples, >95% of the total concentration is explained by Na, Mg, and Ca. Those elements account for >80% of the total concentration in urban dust deposition samples and >65% of the total concentration in snow dust deposition samples, indicating that a majority of the dust mass deposited along the Wasatch Front is from playas. However, many trace elements are enriched in urban and snow dust deposition samples relative to playas. The enrichment diagram (Fig. 6) highlights significant

enrichment in Cu, Se, Ag, Cd, Sb, and La in many deposition samples, each of which has specific urban sources.

Copper in urban areas is sourced from manufacturing and electronic equipment production and waste (Lincoln et al., 2007; Wong et al., 2007; Ajmone-Marsan and Biasioli, 2010), as well as in gasoline, car components, and oil lubricants (Li et al., 2001). Another major source of anthropogenic copper contamination in Utah may be from local mining industries. The Kennecott Copper Mine, one of the largest open-pit copper mines in the world, is located in the Oquirrh Mountains directly south of the GSL (Fig. 1). Tailings piles, dirt roads, and mining operations proximal to and downwind of SLC and Ogden may contribute to the 40-50% higher concentrations observed in those cities relative to Provo and Logan (Table 1). Other mines also exist throughout western Utah that could contribute to the observed Cu enrichment (Reynolds et al., 2014).

Anthropogenic sources of Se such as industrial processes and fossil fuel combustion account for >65% of total Se emissions (Wen and Carignan, 2007). Of the total anthropogenic input, the majority is from coal combustion and Cu refining and smelting (Mosher and Duce, 1987). Silver has been found to correlate with Se, potentially because they both are associated with volatile compounds producing small particles from coal combustion (Salmon et al., 1978; Lee et al., 1994).

Enriched Cd in dust and water is extremely harmful in human and animal kidneys and in marine organisms, where aqueous Cd bioaccumulates. The majority of Cd in air emissions from urban areas is sourced from smelting/metallurgical processing and incineration of wastes (Fishbein L, 1981). Other sources include coating and plating in plastics, production of automobile radiators, and wear and emissions from tires, fuel, and oils (Fishbein L, 1981;

Ajmone-Marsan and Biasioli, 2010). Similarly to Cd, Sb is a possible human carcinogen which can cause a variety of human health concerns if breathed or ingested consistently. Antimony is commonly derived from automotive brake abrasion dust and ash from waste incineration, and it is correlated well with urban Pb and Zn sources (Dietl et al., 1997; van Velzen et al., 1998; von Uexküll et al., 2005; Iijima et al., 2009).

Lanthanum, along with Y, V, and other rare earth elements, is primarily sourced from and oil refineries and is used to determine relative contributions of fuel and oil combustion sources compared with refinery and petrochemical emissions (Olmez and Gordon, 1985; Kulkarni et al., 2006; Moreno et al., 2008, 2010). Typical La/Ce ratios in natural crustal rock ranges from 0.4 to 0.6 (Rudnick and Gao, 2003; Moreno et al., 2010), and increases in the ratio are due to excess La from urban emissions. La/Ce ratios determined in Utah dust are 0.52, 2.10, 0.58, and 0.55 for Provo, SLC, Ogden, and Logan, respectively. This four-fold enrichment of the La/Ce ratio in SLC indicates that there are point sources of La such as refineries in SLC that are not found in other Wasatch Front cities.

To estimate dust contributions from playa sources relative to urban aerosol sources, a mass mixing model was created. Assuming that the total dust mass deposited along the Wasatch Front is the sum of playa dust mass and urban aerosol mass, then for a given element X,

$$Conc_{X\_Playa} * Mass_{Playa} + Conc_{X\_UrbanAerosol} * Mass_{UrbanAerosol} = Conc_{X\_Total} * Mass_{Total}$$

where $Conc_{X\_Total}$ is the concentration of element X in a dust deposition sample and $Mass_{Total}$ is the mass of a dust deposition sample. For pure urban aerosol concentrations, we used data collected from high-volume air samplers in central Barcelona, Spain (Moreno et al., 2006). Assuming similar urban aerosol element concentrations between the Wasatch Front and Barcelona, the relative mas contribution from playas was estimated based on average playa and

average urban dust concentrations of Ti, V, Cr, Mn, Ni, Cu, Se, Mo, Cd, Sb, and Ba. Playa dust contribution estimates for specific elements range from 47-98%, with a mean of 91%. From these results, we conclude that the large majority of the dust mass deposited along the Wasatch Front is sourced from regional playas.

*5.2 Dust Deposition Flux Rates and Chemistry Vary by Season and Location*

Differences in dust fluxes and element concentrations between sampling periods at urban locations indicate seasonal dust differences. Dust flux rates of 24-35g/$m^2$/yr observed in Utah is higher than in other parts of the USA, but lower than major global dust areas. Dust accumulation rates in the southwestern US varied from 2-20 g/$m^2$/yr from 1984 to 1999 (Reheis, 2006), and 5-10 g/$m^2$/yr in the San Juan Mountains snowpack in Colorado (Lawrence et al., 2010). In the Negev Desert, Israel, however, dust accumulation rates have ranged from 120-300 g/$m^2$/yr (Offer and Goossens, 2001). In our samples, there was generally higher flux rates in spring months, suggesting an increased frequency and/or intensity of dust storms (Jewell and Nicoll, 2011; Hahnenberger and Nicoll, 2012). SLC and Ogden flux rates were higher than those at Provo and Logan, suggesting a greater influence of playa and/or urban dust to those locations. SLC has the highest population in Utah, the most industry, and is most proximal to the Kennecott Copper Mine, potentially explaining the high concentrations of elements such as Co, Zn, Cu, Ag, Pb, and most rare earth elements (Table 1). Ogden dust, however, has the lowest concentration for most elements, but the highest concentration of Na, suggesting that its high dust flux is from natural playa dust sources, rather than a large anthropogenic urban source. Furthermore, Ogden is most proximal to the Great Salt Lake and is likely to collect more nearby playa sediments.

The spike in Sr and Na and dip in Co and Se during the January to March sampling period suggests a larger input of playa dust and a dilution of urban dust (Fig. 9). Specifically,

there was a large dust event on February 18, 2018, significantly decreasing visibility in urban Utah. This event darkened mountain snowpack and the local avalanche center reported avalanches from this dusty snow layer. This dust event, among others during the January through March 2018 months, likely caused increased concentrations of Sr and Na, and diluted the concentrations of urban-sourced elements such as Co and Se. The load of Na and Sr, defined as its concentration times dust mass, at all locations was highest in the January-March 2018, and the total load of Co and Se were similar to other seasons.

*5.3 Environmentally Available Elements and Implications for Human and Ecosystem Health*

Each leach step reacts with a different suite of minerals and associated elements, indicating the relative environmental availability of each element. Environmental availability is a term we used to describe the proportion of different minerals and elements that can be absorbed into human, animal, and plant bodies. This absorption can happen through inhalation of dust particles and subsequent dissolving into the bloodstream, and through ingestion of dissolved material in drinking water, for example. The highly environmental available fraction is represented by a combination of the ammonium acetate and acetic acid leach steps (Dastrup et al., 2018). Minerals dissolved in these leach steps include evaporite minerals such as halite and gypsum in the ammonium acetate leach and carbonate minerals such as calcite, aragonite, and dolomite in the acetic acid leach. Because playas have higher concentrations of those minerals compared with urban and snow dust samples, elements commonly found in those minerals such as Na, B, Ca, Sr, and U have high (>50%) bioavailability fractions (Fig. 10). In urban and snow samples, evaporite and carbonate minerals are generally less abundant (Fig. 3), likely resulting from mineral dissolution during transport. Additionally, Se and Cd have high environmental availability (>60%) in fine playa, urban, and snow dust samples (Fig. 10), indicating that both

playa-associated forms of Cd and Se and anthropogenically-sourced Cd and Se are environmentally available.

Immobile elements (Ti, Fe, Cr, Cs) also play an important role in the ecosystem because they aid in soil formation (Lawrence et al., 2013; Dastrup et al., 2018). They will accumulate in soils rather than being dissolved in aquatic systems. On geologic time scales, large accumulations of soils with anomalously high concentrations of metals such as Ti, Cr, Ni and other elements have been attributed to dust deposition rather than local bedrock weathering (Lawrence et al., 2013; Munroe, 2014).

## 6. Conclusion

Dust deposition in Utah, USA represents a mixture of natural playa material and urban anthropogenic contamination. The mineral suite of silicate, carbonate, and evaporite minerals found in central Utah playa dust is the same as that of urban and mountain snowpack dusts. Playas are enriched in Ca, Li, Mg, Na, Sr, and U, which are common constituents in evaporite and carbonate minerals. Dust deposition is enriched in many minor and trace elements, including Cu, Se, Ag, Cd, Sb, and La, which are sourced from industrial activity, mining, and vehicle wear. According to calculations from mass-balance modeling, the contribution from playas relative to urban aerosols is the majority of the dust mass deposited along the Wasatch Front in Utah. Dust deposition flux rates were greatest in the spring, but the element concentrations remained fairly constant. However, a spike in Na and Sr concentrations and a dip in Co and Se during the January-March 2018 sampling period may represent an increased flux of playa dust. Many natural elements exhibit high levels of environment availability in addition to potentially harmful elements such as Cd and Se. By comparing dust sources with dust deposition in a major urban

area, our study has implications for understanding dust transport mechanisms from source to sink and understanding the major components of urban aerosol contamination.

## 7. Tables

Table 1: Total average concentrations (ppm) and standard deviations for fine playa, snow, Provo, SLC, Ogden, and Logan dust samples

| | Avg fine playa | Stdev | Avg Snow | Stdev | Avg Provo | Stdev | Avg SLC | Stdev | Avg Ogden | Stdev | Avg Logan | Stdev |
|---|---|---|---|---|---|---|---|---|---|---|---|---|
| Li | 57.7 | 33.1 | 22.3 | 12.4 | 18.3 | 7.2 | 19.3 | 9.9 | 19.8 | 15.3 | 25.6 | 24.3 |
| Be | 0.20 | 0.13 | 0.55 | 0.15 | 0.49 | 0.21 | 0.43 | 0.17 | 0.38 | 0.07 | 0.42 | 0.10 |
| B | 148.5 | 140.8 | 40.3 | 65.4 | 168.5 | 145.6 | 131.4 | 87.1 | 120.4 | 124.9 | 157.3 | 108.0 |
| Na | 96378 | 108002 | 4252 | 7990 | 21349 | 14392 | 28805 | 10277 | 34078 | 31689 | 24094 | 20825 |
| Mg | 24433 | 10013 | 12651 | 4162 | 13194 | 3800 | 14200 | 3933 | 11152 | 4724 | 17909 | 6677 |
| Al | 2620 | 1691 | 7517 | 2700 | 5843 | 1627 | 5271 | 2448 | 4645 | 1216 | 5032 | 1200 |
| K | 4067 | 4392 | 2553 | 1273 | 5101 | 2804 | 3987 | 1368 | 4759 | 3226 | 5339 | 2443 |
| Ca | 124646 | 73976 | 29362 | 15112 | 71487 | 29167 | 75709 | 38751 | 47579 | 20689 | 72231 | 35893 |
| Ti | 89.7 | 64.3 | 323.9 | 142.6 | 190.4 | 66.6 | 151.6 | 71.6 | 141.6 | 60.8 | 163.0 | 65.3 |
| V | 8.97 | 4.73 | 17.45 | 8.19 | 18.62 | 6.08 | 16.56 | 8.72 | 12.76 | 5.07 | 14.45 | 4.83 |
| Cr | 19.7 | 75.2 | 10.7 | 7.0 | 23.0 | 14.7 | 24.3 | 17.4 | 13.7 | 4.2 | 29.4 | 12.4 |
| Mn | 153 | 93 | 308 | 109 | 347 | 128 | 305 | 152 | 279 | 83 | 403 | 145 |
| Fe | 3936 | 2919 | 10664 | 5630 | 10897 | 4629 | 8828 | 5521 | 8070 | 3309 | 8918 | 3767 |
| Co | 2.51 | 1.70 | 4.82 | 1.70 | 5.00 | 1.28 | 5.01 | 2.78 | 4.25 | 1.09 | 3.89 | 0.91 |
| Ni | 12.3 | 30.5 | 10.1 | 4.4 | 25.6 | 33.4 | 17.5 | 16.2 | 11.7 | 3.9 | 11.6 | 4.7 |
| Cu | 20.3 | 22.0 | 90.6 | 130.0 | 104.9 | 36.4 | 147.1 | 106.7 | 154.6 | 46.1 | 92.8 | 52.9 |
| Zn | | | 121 | 85 | 674 | 499 | 788 | 985 | 474 | 344 | 607 | 487 |
| As | 14.2 | 9.2 | 9.7 | 5.7 | 15.0 | 7.5 | 13.5 | 6.4 | 13.2 | 6.6 | 12.5 | 8.0 |
| Se | 0.34 | 0.46 | 0.33 | 0.42 | 2.35 | 2.08 | 1.81 | 1.45 | 1.58 | 1.34 | 1.71 | 1.12 |
| Rb | 15.24 | 10.25 | 18.29 | 8.07 | 14.16 | 4.44 | 12.82 | 5.15 | 13.74 | 5.27 | 12.89 | 4.95 |
| Sr | 1320 | 945 | 143 | 105 | 309 | 119 | 295 | 100 | 197 | 86 | 230 | 111 |
| Y | 3.48 | 2.12 | 7.33 | 2.20 | 6.71 | 2.36 | 6.49 | 3.62 | 5.93 | 1.79 | 5.95 | 1.26 |
| Mo | 20.39 | 54.66 | 2.75 | 4.54 | 4.03 | 1.99 | 3.97 | 1.82 | 4.55 | 2.31 | 3.64 | 2.23 |
| Ag | 0.07 | 0.08 | 0.17 | 0.20 | 0.22 | 0.11 | 0.48 | 0.76 | 0.23 | 0.12 | 0.17 | 0.08 |
| Cd | 0.24 | 0.16 | 0.52 | 0.32 | 0.96 | 0.49 | 0.93 | 0.70 | 0.95 | 0.48 | 0.74 | 0.37 |
| Sb | 0.93 | 1.17 | 1.20 | 1.36 | 4.77 | 2.68 | 5.56 | 3.52 | 5.64 | 2.23 | 4.87 | 2.83 |
| Cs | 1.88 | 1.62 | 2.17 | 0.99 | 1.40 | 0.60 | 1.37 | 0.87 | 1.19 | 0.53 | 1.12 | 0.48 |
| Ba | 144 | 76 | 149 | 54 | 262 | 100 | 259 | 161 | 201 | 99 | 211 | 86 |
| La | 4.82 | 3.36 | 11.88 | 4.34 | 10.59 | 3.53 | 38.98 | 47.73 | 8.92 | 3.05 | 8.80 | 2.32 |
| Ce | 10.10 | 7.26 | 23.71 | 8.46 | 20.52 | 6.33 | 18.58 | 9.77 | 15.31 | 4.72 | 16.04 | 3.41 |
| Pr | 1.22 | 0.86 | 2.79 | 0.95 | 2.42 | 0.80 | 2.00 | 1.03 | 1.84 | 0.56 | 1.93 | 0.45 |
| Nd | 4.67 | 3.29 | 10.64 | 3.59 | 9.26 | 3.06 | 7.88 | 4.09 | 7.13 | 2.19 | 7.49 | 1.76 |
| Sm | 0.91 | 0.63 | 2.02 | 0.66 | 1.71 | 0.58 | 1.53 | 0.86 | 1.38 | 0.45 | 1.43 | 0.35 |

| | | | | | | | | | | | | |
|---|---|---|---|---|---|---|---|---|---|---|---|---|
| Eu | 0.17 | 0.11 | 0.35 | 0.12 | 0.34 | 0.11 | 0.31 | 0.16 | 0.28 | 0.09 | 0.28 | 0.07 |
| Gd | 0.81 | 0.54 | 1.76 | 0.59 | 1.55 | 0.54 | 1.37 | 0.74 | 1.26 | 0.40 | 1.29 | 0.30 |
| Tb | 0.11 | 0.07 | 0.24 | 0.08 | 0.22 | 0.08 | 0.19 | 0.11 | 0.18 | 0.06 | 0.18 | 0.04 |
| Dy | 0.65 | 0.42 | 1.35 | 0.45 | 1.17 | 0.38 | 1.08 | 0.54 | 1.02 | 0.35 | 1.05 | 0.25 |
| Ho | 0.12 | 0.08 | 0.24 | 0.08 | 0.22 | 0.08 | 0.20 | 0.11 | 0.19 | 0.07 | 0.20 | 0.05 |
| Er | 0.34 | 0.21 | 0.68 | 0.23 | 0.62 | 0.23 | 0.57 | 0.32 | 0.53 | 0.18 | 0.54 | 0.13 |
| Yb | 0.28 | 0.18 | 0.55 | 0.19 | 0.47 | 0.16 | 0.44 | 0.22 | 0.43 | 0.17 | 0.43 | 0.12 |
| Lu | 0.04 | 0.03 | 0.08 | 0.03 | 0.08 | 0.03 | 0.07 | 0.04 | 0.07 | 0.02 | 0.07 | 0.02 |
| Tl | 0.21 | 0.28 | 0.19 | 0.13 | 0.22 | 0.09 | 0.17 | 0.09 | 0.16 | 0.06 | 0.14 | 0.05 |
| Pb | | | 31.2 | 27.1 | 36.2 | 17.0 | 47.0 | 39.4 | 33.3 | 12.3 | 21.9 | 7.3 |
| Th | 1.62 | 1.29 | 4.41 | 1.67 | 3.19 | 2.36 | 2.94 | 2.83 | 2.61 | 1.40 | 2.14 | 1.16 |
| U | 2.72 | 1.72 | 1.02 | 0.40 | 0.94 | 0.30 | 0.82 | 0.38 | 0.64 | 0.18 | 0.61 | 0.20 |

Table 2: Urban dust deposition flux rates

| Sample ID | Location | Sampling Months | Collection period (days) | Total dust weight (g) | Dust Flux ($g/m^2/yr$) |
|---|---|---|---|---|---|
| 12456 | Ogden | Sep-Nov 2015 | 63 | 0.410 | 0.74 |
| 12457 | SLC | Sep-Nov 2015 | 63 | 0.534 | 0.97 |
| 12458 | Provo | Sep-Nov 2015 | 63 | 0.275 | 0.50 |
| 12459 | Logan | Sep-Nov 2015 | 63 | 0.350 | 0.63 |
| 12460 | Provo 2 wk | Sep-Nov 2015 | 8 | 0.137 | 1.96 |
| 12653 | Provo | Feb-May 2016 | 75 | 0.974 | 1.48 |
| 12654 | Provo 2 wk | Feb-May 2016 | 18 | 0.291 | 1.85 |
| 12655 | SLC | Feb-May 2016 | 75 | 1.531 | 2.33 |
| 12656 | Logan | Feb-May 2016 | 75 | 1.240 | 1.89 |
| 13662 | Ogden | Jun-Aug 2017 | 61 | 0.799 | 1.50 |
| 13663 | Logan | Jun-Aug 2017 | 61 | 0.723 | 1.35 |
| 13820 | Provo | Aug-Oct 2017 | 59 | 0.941 | 1.82 |
| 13821 | SLC | Aug-Oct 2017 | 59 | 1.345 | 2.61 |
| 13822 | Ogden | Aug-Oct 2017 | 59 | 1.208 | 2.34 |
| 13823 | Logan | Aug-Oct 2017 | 59 | 0.966 | 1.87 |
| 13886 | Provo | Oct-Jan 2017-2018 | 77 | 0.975 | 1.45 |
| 13887 | SLC | Oct-Jan 2017-2018 | 77 | 1.745 | 2.59 |
| 13888 | Ogden | Oct-Jan 2017-2018 | 77 | 1.850 | 2.75 |
| 13889 | Logan | Oct-Jan 2017-2018 | 77 | 1.007 | 1.50 |
| 13981 | Provo | Jan-Mar 2018 | 60 | 1.397 | 2.66 |
| 13982 | SLC | Jan-Mar 2018 | 60 | 1.773 | 3.38 |
| 13983 | Ogden | Jan-Mar 2018 | 60 | 1.373 | 2.62 |
| 13984 | Logan | Jan-Mar 2018 | 60 | 1.159 | 2.21 |
| 14120 | Provo | Mar-May 2018 | 62 | 1.666 | 3.07 |

| | | | | | |
|---|---|---|---|---|---|
| 14121 | SLC | Mar-May 2018 | 62 | 1.449 | 2.67 |
| 14122 | Ogden | Mar-May 2018 | 62 | 2.088 | 3.85 |
| 14123 | Logan | Mar-May 2018 | 62 | 1.075 | 1.98 |
| 14124 | Provo | May-July 2018 | 61 | 1.091 | 2.04 |
| 14125 | SLC | May-July 2018 | 61 | 1.930 | 3.62 |
| 14126 | Ogden | May-July 2018 | 61 | 1.738 | 3.26 |
| 14127 | Logan | May-July 2018 | 61 | 1.223 | 2.29 |
| 14231 | Provo | Jul-Sep 2018 | 63 | 1.8103 | 3.29 |
| 14232 | SLC | Jul-Sep 2018 | 63 | 1.3483 | 2.45 |
| 14233 | Ogden | Jul-Sep 2018 | 63 | 1.0138 | 1.84 |
| 14234 | Logan | Jul-Sep 2018 | 63 | 1.3667 | 2.48 |

8. Figures

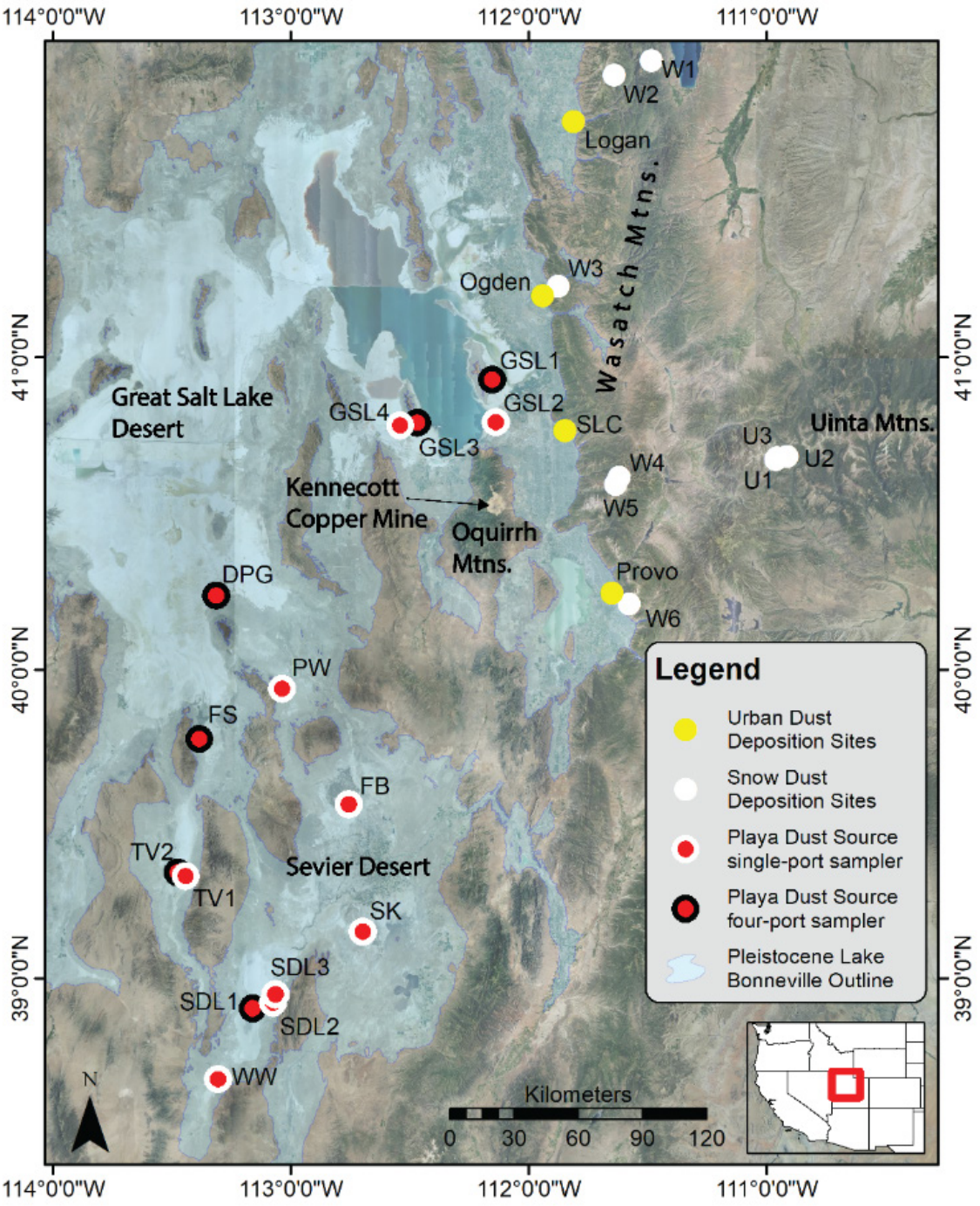


Figure 1: Playa, urban, and snow dust sampling locations in Utah, USA. Playa dust source samplers were located in dry lakebeds that are the remnant of Lake Bonneville, including the Great Salt Lake lakebed. Urban dust deposition samplers were placed on rooftops of buildings, and snow samples were collected from pits dug in mountain snowpack.

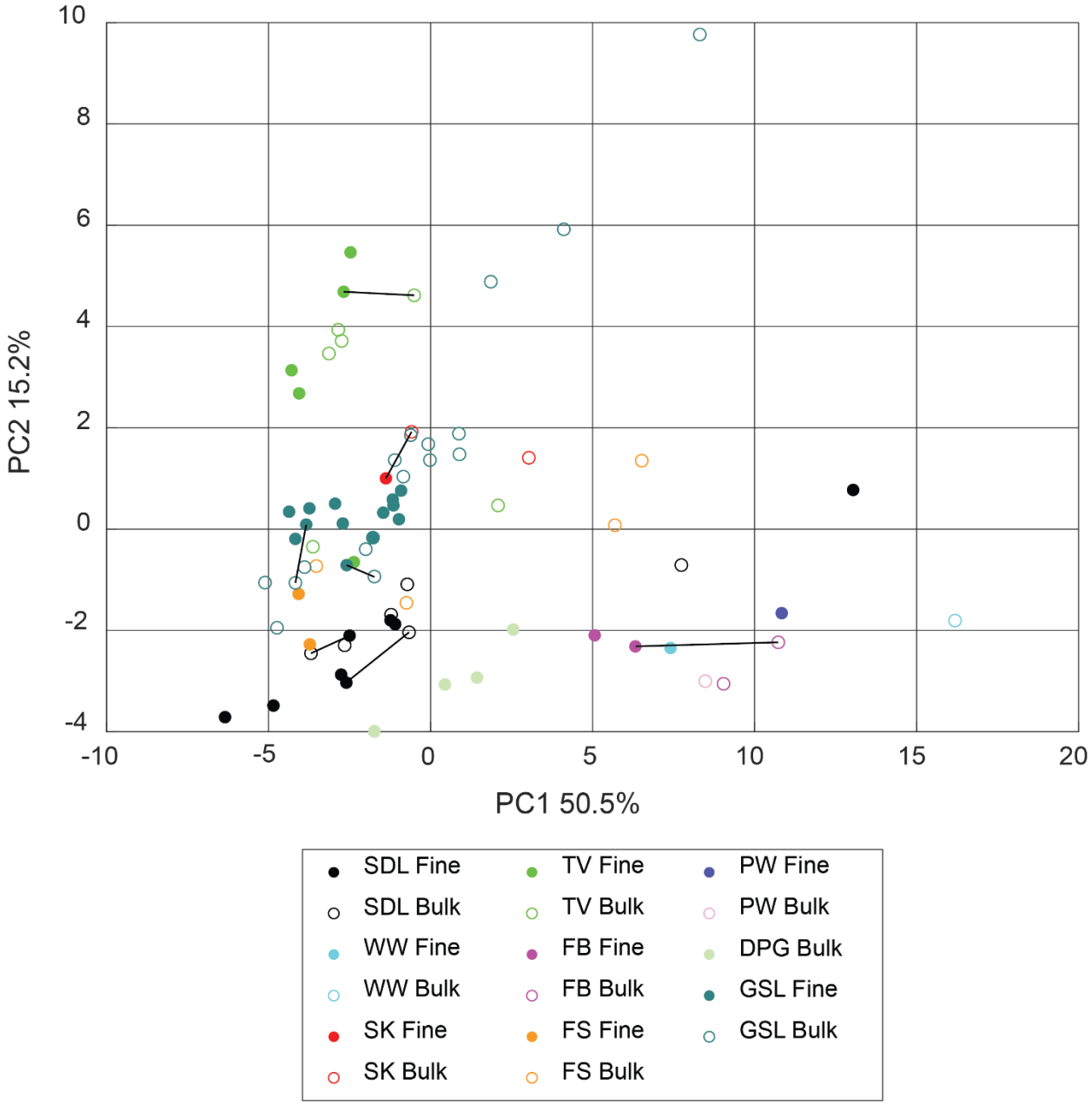


Figure 2: PCA of all dust source samples based on the total concentrations of all elements. Principal component 1 (PC1) explains 50.5% of the total variance and is primarily explained by Be, Al, Mn, Fe, Co, Y, REE's, and Th. Principal component 2 (PC2) explains 15.2% of the total variance and is primarily explained by Li, B, As, Se, Rb, Sr, Cd, Cs, and U. Tie lines represent the sieved and bulk fractions of the same sample analyzed separately.

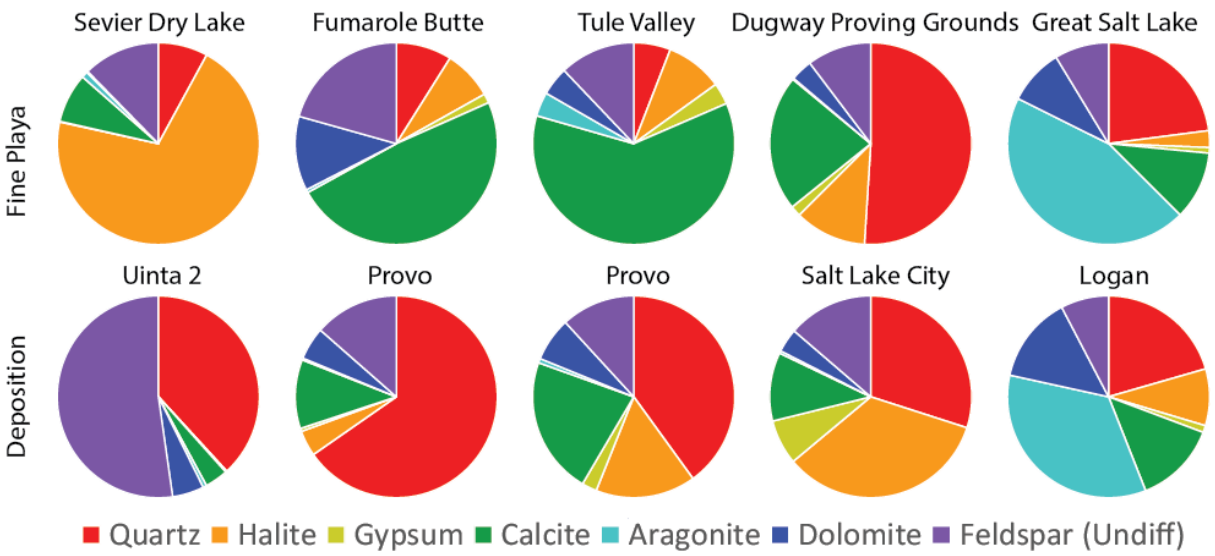


Figure 3: Mineral composition of 10 samples based on the reference intensity ratio (RIR) analysis of x-ray diffraction (XRD) patterns. Although mineral abundances between samples vary greatly, the suite of minerals is the same for all samples.

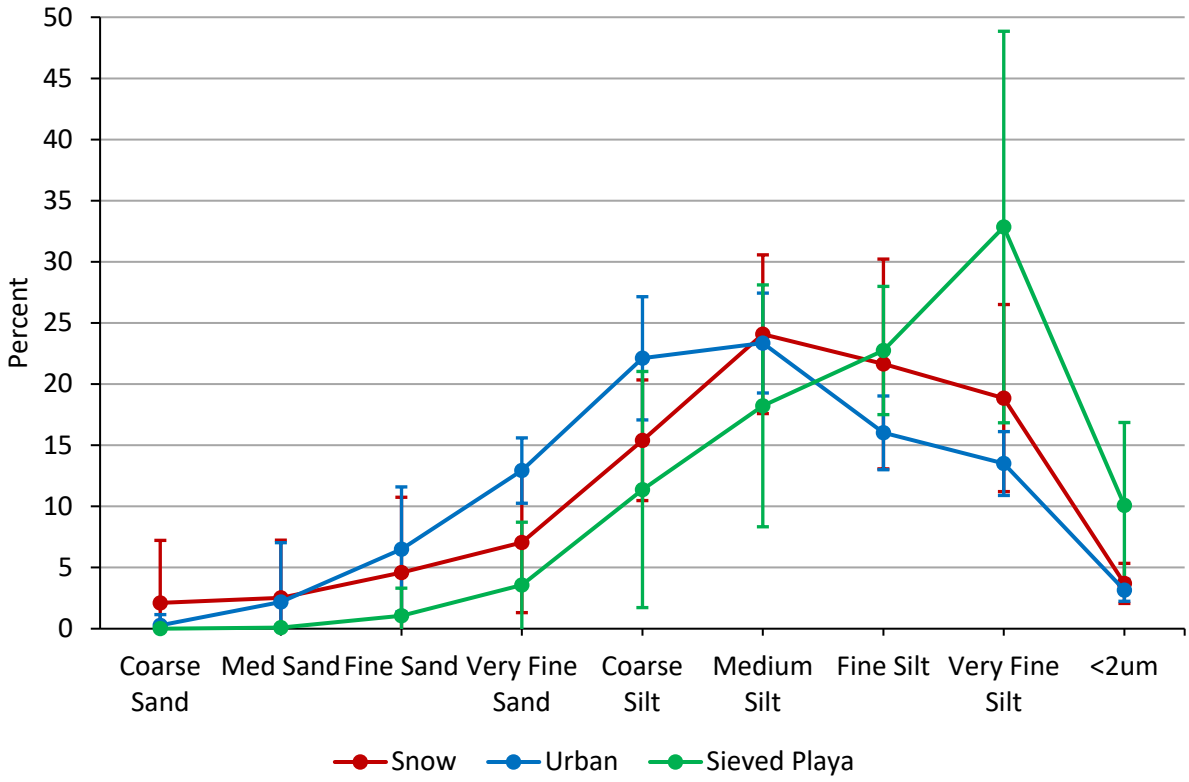


Figure 4: Grain size analysis of snow, urban, and sieved playa samples. Ten of each sample type were analyzed, and averages and are shown for each size fraction. Within error, snow, urban, and sieved playa samples have the same grain-size distribution. Error bars represent one standard deviation.

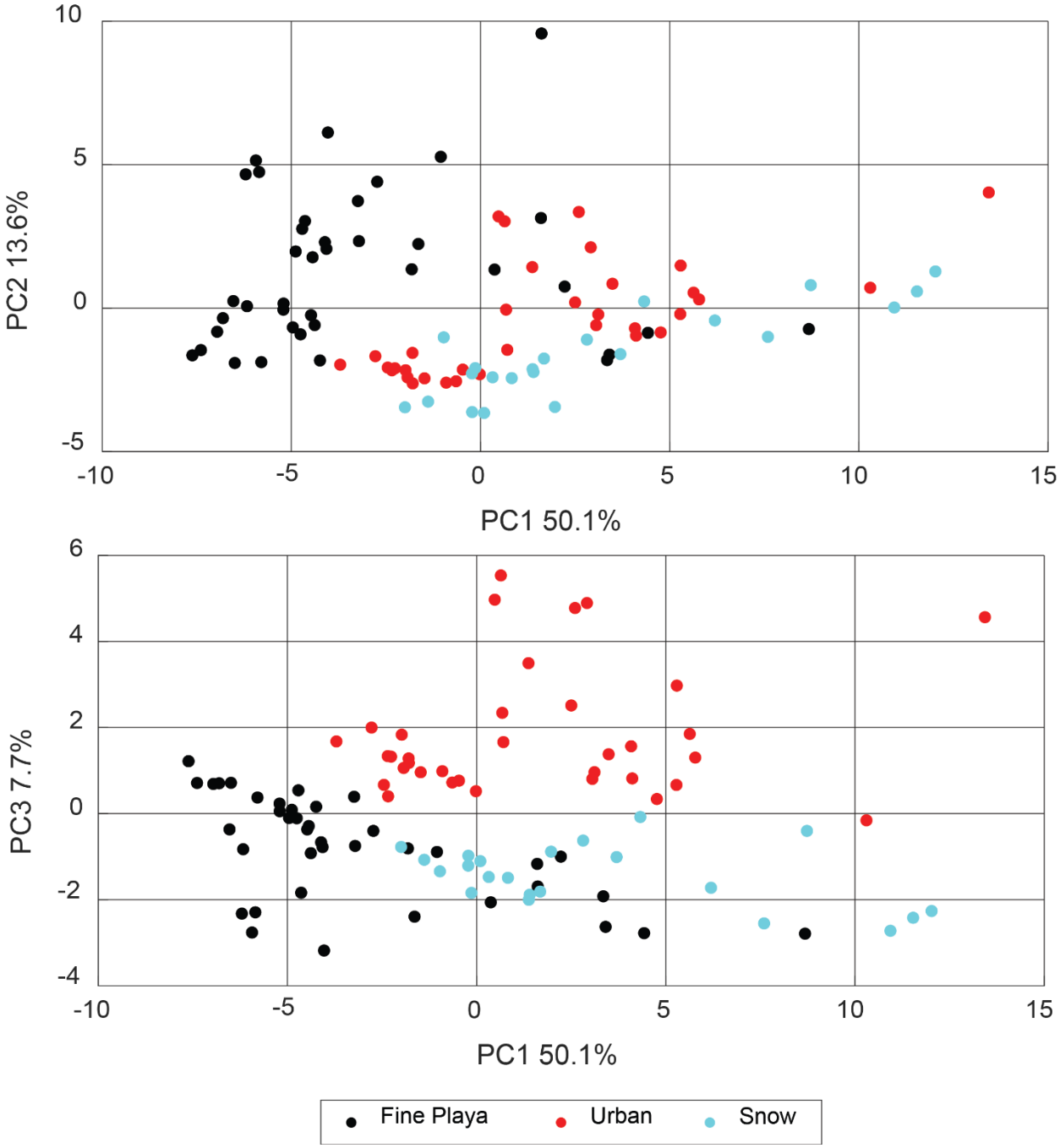


Figure 5: PCA on all fine playa, urban, and snow dust samples based on the total concentration of all elements. The top panel shows PC1 vs. PC2, where PC1 accounts for 50.1% of the total variance and is primarily explained by Be, Al, V, Mn, Fe, Co, Y, REE's, and Th, while PC2 accounts for 12.0% of the total variance and is primarily explained by B, Mg, Ca, As, Rb, Sr, Cs, and U. The bottom panel shows PC1 vs PC3, where PC3 accounts for 7.7% of the variance and is characteristic of Se, Cd, and Sb.

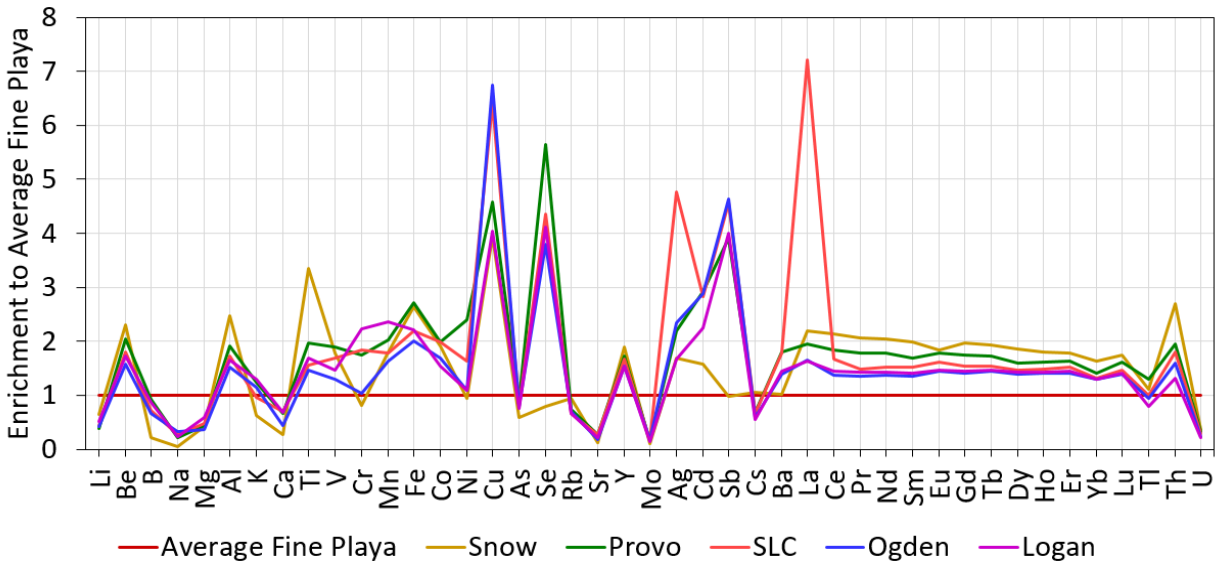


Figure 6: Enrichment diagram comparing average concentrations of snow, Provo, SLC, Ogden, and Logan with average fine playa samples. Substantial depletion is observed in Na, Mg, Ca, Sr, Mo, Cs, and U, and substantial enrichment is observed in Cu, Se, Ag, Cd, Sb, and La.

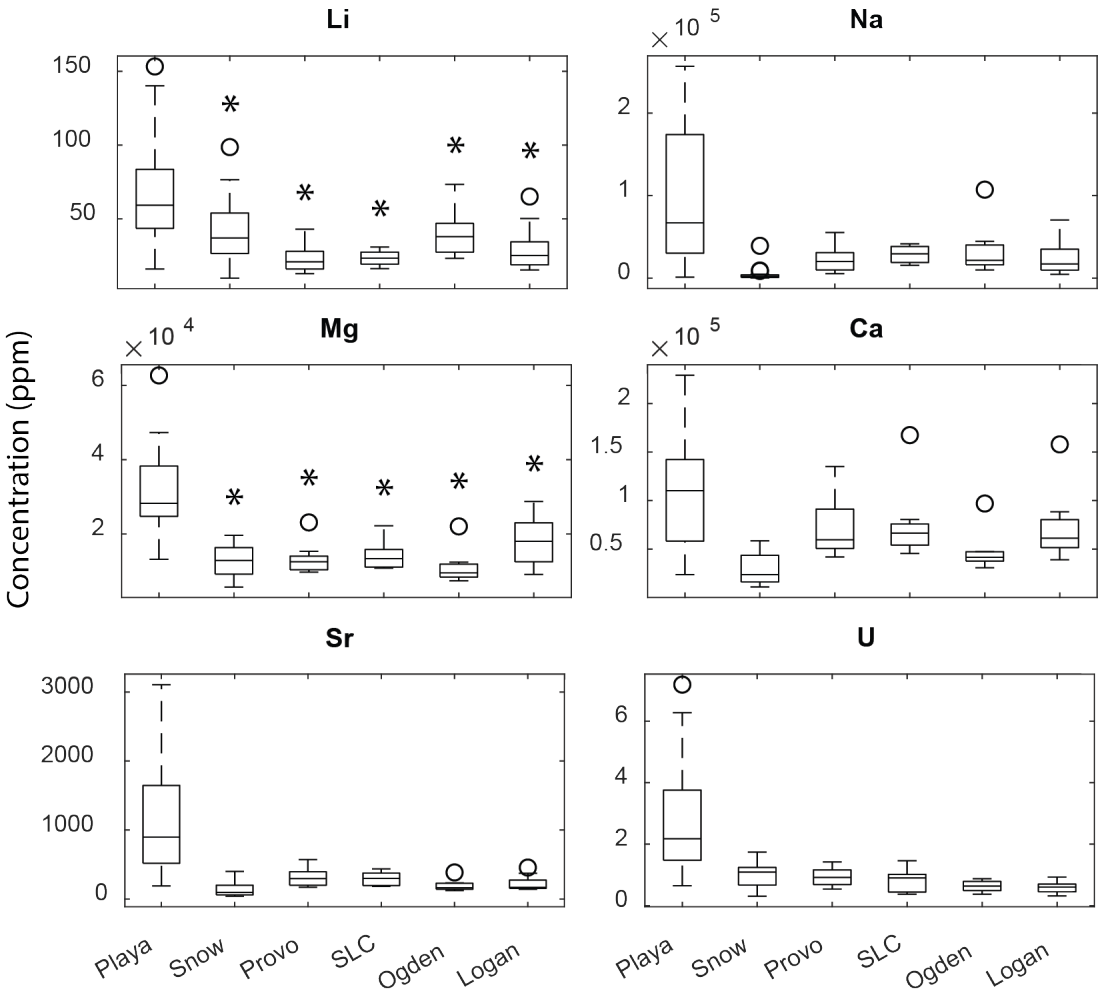


Figure 7: Box plots showing fine playa, snow, Provo, SLC, Ogden, and Logan dust concentrations of playa-associated elements. Asterisks indicate statistically significant depletion with 95% confidence.

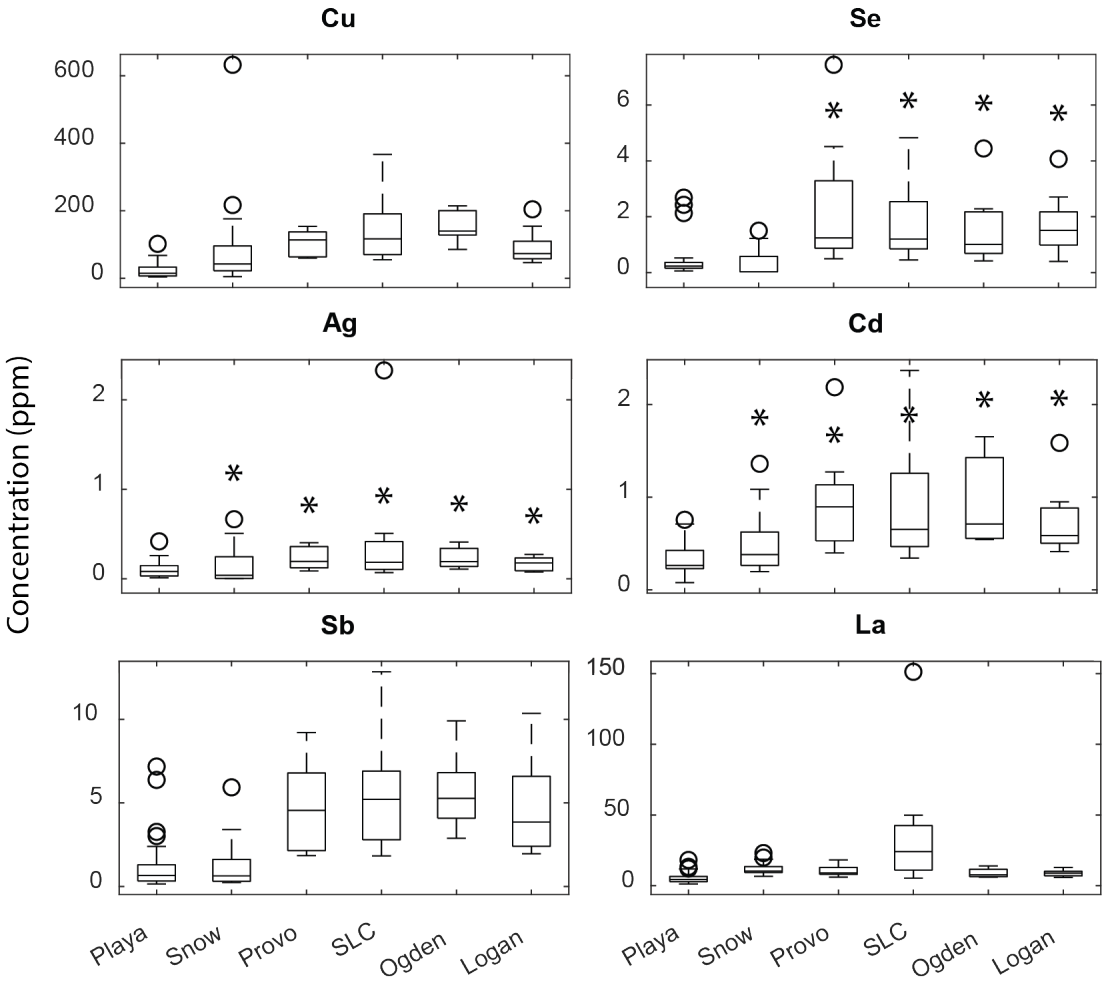


Figure 8: Box plots showing fine playa, snow, Provo, SLC, Ogden, and Logan concentrations of elements sourced from urban anthropogenic sources. Asterisks indicate statistically significant enrichment at 95% confidence.

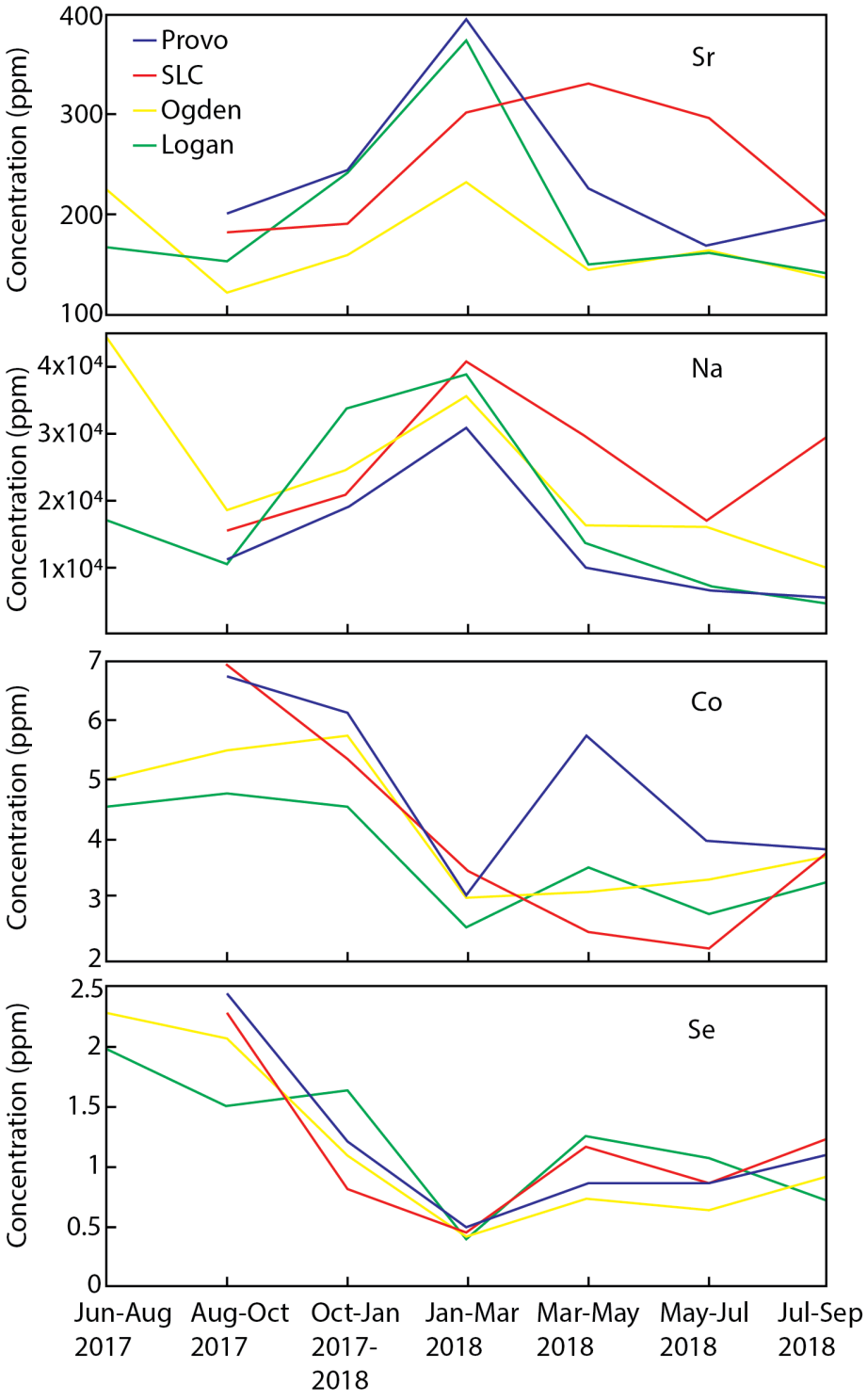


Figure 9: Time series comparison of the total concentrations of Sr, Na, Co, and Se. In the Jan-Mar 2018 sample, an increase in Sr and Na suggests increased input from playa dust sources. A corresponding decrease in Co and Se represents a dilution effect of urban-sourced elements.

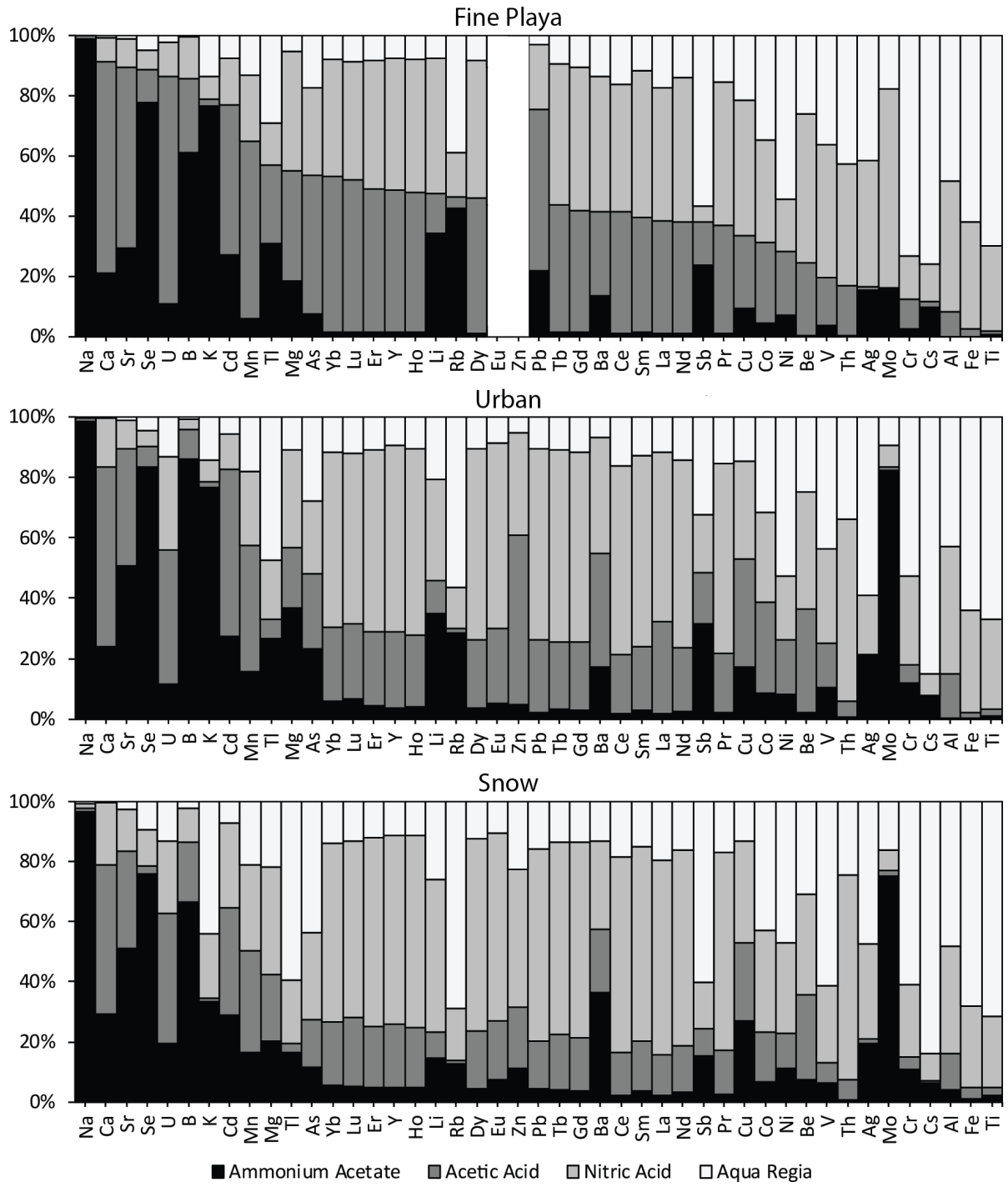


Figure 10: Leaching results for urban, snow, and playa samples. Higher percent contributions from the first two leach steps (ammonium acetate and acetic acid) represents the highly bioavailable fraction, or the fraction easily dissolved and consumed by humans, animals, and plants. In all sample types, potentially harmful elements Cd and Se exhibit >60% bioavailability.

9. References

Aarons, S.M., Blakowski, M.A., Aciego, S.M., Stevenson, E.I., Sims, K.W.W., Scott, S.R., and Aarons, C., 2017, Geochemical characterization of critical dust source regions in the American West: Geochimica et Cosmochimica Acta, v. 215, p. 141–161, doi:10.1016/j.gca.2017.07.024.

Abed, A.M., Al Kuisi, M., and Khair, H.A., 2009, Characterization of the Khamaseen (spring) dust in Jordan: Atmospheric Environment, v. 43, p. 2868–2876, doi:10.1016/j.atmosenv.2009.03.015.

Ajmone-Marsan, F., and Biasioli, M., 2010, Trace Elements in Soils of Urban Areas: Water, Air, & Soil Pollution, v. 213, p. 121–143, doi:10.1007/s11270-010-0372-6.

Bartholet, J., 2012, SWEPT FROM AFRICA TO THE AMAZON: Scientific American, v. 306, p. 44–49.

Ben-Israel, M., Enzel, Y., Amit, R., and Erel, Y., 2015, Provenance of the various grain-size fractions in the Negev loess and potential changes in major dust sources to the Eastern Mediterranean: Quaternary Research, v. 83, p. 105–115, doi:10.1016/j.yqres.2014.08.001.

Brahney, J., Mahowald, N., Ward, D.S., Ballantyne, A.P., and Neff, J.C., 2015, Is atmospheric phosphorus pollution altering global alpine Lake stoichiometry? Global Biogeochemical Cycles, v. 29, p. 1369–1383, doi:10.1002/2015GB005137.

Cahill, T.A., Gill, T.E., Reid, J.S., Gearhart, E.A., and Gillette, D.A., 1996, Saltating Particles, Playa Crusts and Dust Aerosols at Owens (dry) Lake, California: Earth Surface Processes and Landforms, v. 21, p. 621–639, doi:10.1002/(SICI)1096-9837(199607)21:7<621::AID-ESP661>3.0.CO;2-E.

Carling, G.T., Fernandez, D.P., and Johnson, W.P., 2012, Dust-mediated loading of trace and major elements to Wasatch Mountain snowpack: Science of The Total Environment, v. 432, p. 65–77, doi:10.1016/j.scitotenv.2012.05.077.

Das, R., Khezri, B., Srivastava, B., Datta, S., Sikdar, P.K., Webster, R.D., and Wang, X., 2015, Trace element composition of PM2.5 and PM10 from Kolkata – a heavily polluted Indian metropolis: Atmospheric Pollution Research, v. 6, p. 742–750, doi:10.5094/APR.2015.083.

Dastrup, D.B., Carling, G.T., Collins, S.A., Nelson, S.T., Fernandez, D.P., Tingey, D.G., Hahnenberger, M., and Aanderud, Z.T., 2018, Aeolian dust chemistry and bacterial communities in snow are unique to airshed locations across northern Utah, USA: Atmospheric Environment, v. 193, p. 251–261, doi:10.1016/j.atmosenv.2018.09.016.

Derbyshire, E., 2007, Natural Minerogenic Dust and Human Health: AMBIO: A Journal of the Human Environment, v. 36, p. 73–77, doi:10.1579/0044-7447(2007)36[73:NMDAHH]2.0.CO;2.

Dietl, C., Reifenhäuser, W., and Peichl, L., 1997, Association of antimony with traffic — occurrence in airborne dust, deposition and accumulation in standardized grass cultures: Science of The Total Environment, v. 205, p. 235–244, doi:10.1016/S0048-9697(97)00204-0.

Divrikli, U., Soylak, M., Elci, L., and Dogan, M., 2003, Trace Heavy Metal Levels in Street Dust Samples from Yozgat City Center, Turkey: Journal of Trace and Microprobe Techniques, v. 21, p. 351–361, doi:10.1081/TMA-120020270.

Fairlie, D.T., Jacob, D.J., and Park, R.J., 2007, The impact of transpacific transport of mineral dust in the United States: Atmospheric Environment, v. 41, p. 1251–1266, doi:10.1016/j.atmosenv.2006.09.048.

Fishbein L, 1981, Sources, transport and alterations of metal compounds: an overview. I. Arsenic, beryllium, cadmium, chromium, and nickel.: Environmental Health Perspectives, v. 40, p. 43–64, doi:10.1289/ehp.814043.

Frie, A.L., Dingle, J.H., Ying, S.C., and Bahreini, R., 2017, The Effect of a Receding Saline Lake (The Salton Sea) on Airborne Particulate Matter Composition: Environmental Science & Technology, v. 51, p. 8283–8292, doi:10.1021/acs.est.7b01773.

Fryrear, D.W., 1986, A field dust sampler: Journal of Soil and Water Conservation, v. 41, p. 117–120.

Gill, T.E., 1996, Eolian sediments generated by anthropogenic disturbance of playas: human impacts on the geomorphic system and geomorphic impacts on the human system: Geomorphology, v. 17, p. 207–228, doi:10.1016/0169-555X(95)00104-D.

Goudie, A.S., 2014, Desert dust and human health disorders: Environment International, v. 63, p. 101–113, doi:10.1016/j.envint.2013.10.011.

Goudie, A.S., 2009, Dust storms: Recent developments: Journal of Environmental Management, v. 90, p. 89–94, doi:10.1016/j.jenvman.2008.07.007.

Gunawardana, C., Goonetilleke, A., Egodawatta, P., Dawes, L., and Kokot, S., 2012, Source characterisation of road dust based on chemical and mineralogical composition: Chemosphere, v. 87, p. 163–170, doi:10.1016/j.chemosphere.2011.12.012.

Hahnenberger, M., and Nicoll, K., 2014, Geomorphic and land cover identification of dust sources in the eastern Great Basin of Utah, U.S.A.: Geomorphology, v. 204, p. 657–672, doi:10.1016/j.geomorph.2013.09.013.

Hahnenberger, M., and Nicoll, K., 2012, Meteorological characteristics of dust storm events in the eastern Great Basin of Utah, U.S.A.: Atmospheric Environment, v. 60, p. 601–612, doi:10.1016/j.atmosenv.2012.06.029.

Hubbard, C.R., Evans, E.H., and Smith, D.K., 1976, The reference intensity ratio, I/Ic, for computer simulated powder patterns: Journal of Applied Crystallography, v. 9, p. 169–174, doi:10.1107/S0021889876010807.

Iijima, A., Sato, K., Fujitani, Y., Fujimori, E., Saito, Y., Tanabe, K., Ohara, T., Kozawa, K., and Furuta, N., 2009, Clarification of the predominant emission sources of antimony in airborne particulate matter and estimation of their effects on the atmosphere in Japan: Environmental Chemistry, v. 6, p. 122–132, doi:10.1071/EN08107.

Jewell, P.W., and Nicoll, K., 2011, Wind regimes and aeolian transport in the Great Basin, U.S.A.: Geomorphology, v. 129, p. 1–13, doi:10.1016/j.geomorph.2011.01.005.

Kellogg, C.A., and Griffin, D.W., 2006, Aerobiology and the global transport of desert dust: Trends in Ecology & Evolution, v. 21, p. 638–644, doi:10.1016/j.tree.2006.07.004.

Kubilay, N., and Saydam, A.C., 1995, Trace elements in atmospheric particulates over the Eastern Mediterranean; Concentrations, sources, and temporal variability: Atmospheric Environment, v. 29, p. 2289–2300, doi:10.1016/1352-2310(95)00101-4.

Kulkarni, P., Chellam, S., and Fraser, M.P., 2006, Lanthanum and lanthanides in atmospheric fine particles and their apportionment to refinery and petrochemical operations in Houston, TX: Atmospheric Environment, v. 40, p. 508–520, doi:10.1016/j.atmosenv.2005.09.063.

Lawrence, C.R., and Neff, J.C., 2009, The contemporary physical and chemical flux of aeolian dust: A synthesis of direct measurements of dust deposition: Chemical Geology, v. 267, p. 46–63, doi:10.1016/j.chemgeo.2009.02.005.

Lawrence, C.R., Painter, T.H., Landry, C.C., and Neff, J.C., 2010, Contemporary geochemical composition and flux of aeolian dust to the San Juan Mountains, Colorado, United States: Journal of Geophysical Research: Biogeosciences, v. 115, p. G03007, doi:10.1029/2009JG001077.

Lawrence, C.R., Reynolds, R.L., Ketterer, M.E., and Neff, J.C., 2013, Aeolian controls of soil geochemistry and weathering fluxes in high-elevation ecosystems of the Rocky Mountains, Colorado: Geochimica et Cosmochimica Acta, v. 107, p. 27–46, doi:10.1016/j.gca.2012.12.023.

Lee, D.S., Garland, J.A., and Fox, A.A., 1994, Atmospheric concentrations of trace elements in urban areas of the United Kingdom: Atmospheric Environment, v. 28, p. 2691–2713, doi:10.1016/1352-2310(94)90442-1.

Lee, R.E., Goranson, S.S., Enrione, R.E., and Morgan, G.B., 1972, National Air Surveillance cascade impactor network. II. Size distribution measurements of trace metal components: Environmental Science & Technology, v. 6, p. 1025–1030, doi:10.1021/es60071a002.

Li, X., Poon, C., and Liu, P.S., 2001, Heavy metal contamination of urban soils and street dusts in Hong Kong: Applied Geochemistry, v. 16, p. 1361–1368, doi:10.1016/S0883-2927(01)00045-2.

Lincoln, J.D., Ogunseitan, O.A., Shapiro, A.A., and Saphores, J.-D.M., 2007, Leaching Assessments of Hazardous Materials in Cellular Telephones: Environmental Science & Technology, v. 41, p. 2572–2578, doi:10.1021/es0610479.

Liu, D., Abuduwaili, J., Lei, J., and Wu, G., 2011, Deposition Rate and Chemical Composition of the Aeolian Dust from a Bare Saline Playa, Ebinur Lake, Xinjiang, China: Water, Air, & Soil Pollution, v. 218, p. 175–184, doi:10.1007/s11270-010-0633-4.

Mallia, D.V., Kochanski, A., Wu, D., Pennell, C., Oswald, W., and Lin, J.C., 2017, Wind-Blown Dust Modeling Using a Backward-Lagrangian Particle Dispersion Model: Journal of Applied Meteorology and Climatology, v. 56, p. 2845–2867, doi:10.1175/JAMC-D-16-0351.1.

McTainsh, G., and Strong, C., 2007, The role of aeolian dust in ecosystems: Geomorphology, v. 89, p. 39–54, doi:10.1016/j.geomorph.2006.07.028.

Meza-Figueroa, D., De la O-Villanueva, M., and De la Parra, M.L., 2007, Heavy metal distribution in dust from elementary schools in Hermosillo, Sonora, México: Atmospheric Environment, v. 41, p. 276–288, doi:10.1016/j.atmosenv.2006.08.034.

Moreno, T., Querol, X., Alastuey, A., Pey, J., Minguillón, M.C., Pérez, N., Bernabé, R.M., Blanco, S., Cárdenas, B., and Gibbons, W., 2008, Lanthanoid Geochemistry of Urban Atmospheric Particulate Matter: Environmental Science & Technology, v. 42, p. 6502–6507, doi:10.1021/es800786z.

Moreno, T., Querol, X., Alastuey, A., de la Rosa, J., Sánchez de la Campa, A.M., Minguillón, M., Pandolfi, M., González-Castanedo, Y., Monfort, E., and Gibbons, W., 2010, Variations in vanadium, nickel and lanthanoid element concentrations in urban air: Science of The Total Environment, v. 408, p. 4569–4579, doi:10.1016/j.scitotenv.2010.06.016.

Moreno, T., Querol, X., Alastuey, A., Viana, M., Salvador, P., Sánchez de la Campa, A., Artiñano, B., de la Rosa, J., and Gibbons, W., 2006, Variations in atmospheric PM trace metal content in Spanish towns: Illustrating the chemical complexity of the inorganic urban aerosol cocktail: Atmospheric Environment, v. 40, p. 6791–6803, doi:10.1016/j.atmosenv.2006.05.074.

Mosher, B.W., and Duce, R.A., 1987, A global atmospheric selenium budget: Journal of Geophysical Research: Atmospheres, v. 92, p. 13289–13298, doi:10.1029/JD092iD11p13289.

Munroe, J.S., 2014, Properties of modern dust accumulating in the Uinta Mountains, Utah, USA, and implications for the regional dust system of the Rocky Mountains: Earth Surface Processes and Landforms, v. 39, p. 1979–1988, doi:10.1002/esp.3608.

Munroe, J.S., Attwood, E.C., O'Keefe, S.S., and Quackenbush, P.J.M., 2015, Eolian deposition in the alpine zone of the Uinta Mountains, Utah, USA: CATENA, v. 124, p. 119–129, doi:10.1016/j.catena.2014.09.008.

Neff, J.C., Ballantyne, A.P., Farmer, G.L., Mahowald, N.M., Conroy, J.L., Landry, C.C., Overpeck, J.T., Painter, T.H., Lawrence, C.R., and Reynolds, R.L., 2008, Increasing eolian dust deposition in the western United States linked to human activity: Nature Geoscience, v. 1, p. 189, doi:10.1038/ngeo133.

Offer, Z.Y., and Goossens, D., 2001, Ten years of aeolian dust dynamics in a desert region (Negev desert, Israel): analysis of airborne dust concentration, dust accumulation and the high-magnitude dust events: Journal of Arid Environments, v. 47, p. 211–249, doi:10.1006/jare.2000.0706.

Olmez, I., and Gordon, G.E., 1985, Rare Earths: Atmospheric Signatures for Oil-Fired Power Plants and Refineries: Science, v. 229, p. 966–968, doi:10.1126/science.229.4717.966.

Oviatt, C.G., 1988, Late Pleistocene and Holocene lake fluctuations in the Sevier Lake basin, Utah, USA: Journal of Paleolimnology, v. 1, p. 9–21, doi:10.1007/BF00202190.

Painter, T.H., Deems, J.S., Belnap, J., Hamlet, A.F., Landry, C.C., and Udall, B., 2010, Response of Colorado River runoff to dust radiative forcing in snow: Proceedings of the National Academy of Sciences, v. 107, p. 17125–17130, doi:10.1073/pnas.0913139107.

Perry, K.D., Cahill, T.A., Eldred, R.A., Dutcher, D.D., and Gill, T.E., 1997, Long-range transport of North African dust to the eastern United States: Journal of Geophysical Research: Atmospheres, v. 102, p. 11225–11238, doi:10.1029/97JD00260.

Pope, C.A., Dockery, D.W., Spengler, J.D., and Raizenne, M.E., 1991, Respiratory Health and PM10 Pollution: A Daily Time Series Analysis: American Review of Respiratory Disease, v. 144, p. 668–674, doi:10.1164/ajrccm/144.3_Pt_1.668.

Prospero, J.M., Ginoux, P., Torres, O., Nicholson, S.E., and Gill, T.E., 2002, Environmental Characterization of Global Sources of Atmospheric Soil Dust Identified with the Nimbus 7 Total Ozone Mapping Spectrometer (toms) Absorbing Aerosol Product: Reviews of Geophysics, v. 40, p. 1002, doi:10.1029/2000RG000095.

Reheis, M.C., 2006, A 16-year record of eolian dust in Southern Nevada and California, USA: Controls on dust generation and accumulation: Journal of Arid Environments, v. 67, p. 487–520, doi:10.1016/j.jaridenv.2006.03.006.

Reheis, M.C., 1997, Dust deposition downwind of Owens (dry) Lake, 1991–1994: Preliminary findings: Journal of Geophysical Research: Atmospheres, v. 102, p. 25999–26008, doi:10.1029/97JD01967.

Reheis, M.C., Budahn, J.R., and Lamothe, P.J., 2002, Geochemical evidence for diversity of dust sources in the southwestern United States: Geochimica et Cosmochimica Acta, v. 66, p. 1569–1587, doi:10.1016/S0016-7037(01)00864-X.

Reheis, M.C., Budahn, J.R., Lamothe, P.J., and Reynolds, R.L., 2009, Compositions of modern dust and surface sediments in the Desert Southwest, United States: Journal of Geophysical Research: Earth Surface, v. 114, p. F01028, doi:10.1029/2008JF001009.

Reheis, M.C., and Kihl, R., 1995, Dust deposition in southern Nevada and California, 1984–1989: Relations to climate, source area, and source lithology: Journal of Geophysical Research: Atmospheres, v. 100, p. 8893–8918, doi:10.1029/94JD03245.

Reimann, C., and de Caritat, P., 2005, Distinguishing between natural and anthropogenic sources for elements in the environment: regional geochemical surveys versus enrichment factors: Science of The Total Environment, v. 337, p. 91–107, doi:10.1016/j.scitotenv.2004.06.011.

Reynolds, R.L. et al., 2014, Composition of dust deposited to snow cover in the Wasatch Range (Utah, USA): Controls on radiative properties of snow cover and comparison to some dust-source sediments: Aeolian Research, v. 15, p. 73–90, doi:10.1016/j.aeolia.2013.08.001.

Reynolds, R.L., Yount, J.C., Reheis, M., Goldstein, H., Chavez, P., Fulton, R., Whitney, J., Fuller, C., and Forester, R.M., 2007, Dust emission from wet and dry playas in the Mojave Desert, USA: Earth Surface Processes and Landforms, v. 32, p. 1811–1827, doi:10.1002/esp.1515.

Rudnick, R.L., and Gao, S., 2003, Composition of the Continental Crust: Treatise on Geochemistry, v. 3, p. 659, doi:10.1016/B0-08-043751-6/03016-4.

Salmon, L., Atkins, D.H.F., Fisher, E.M.R., Healy, C., and Law, D.V., 1978, Retrospective trend analysis of the content of U.K. air particulate material 1957–1974: Science of The Total Environment, v. 9, p. 161–199, doi:10.1016/0048-9697(78)90074-8.

Samara, C., and Voutsa, D., 2005, Size distribution of airborne particulate matter and associated heavy metals in the roadside environment: Chemosphere, v. 59, p. 1197–1206, doi:10.1016/j.chemosphere.2004.11.061.

Skiles, S.M., Mallia, D.V., Hallar, A.G., Lin, J.C., Lambert, A., Petersen, R., and Steven Clark, 2018, Implications of a shrinking Great Salt Lake for dust on snow deposition in the Wasatch Mountains, UT, as informed by a source to sink case study from the 13–14 April 2017 dust event: Environmental Research Letters, v. 13, p. 124031, doi:10.1088/1748-9326/aaefd8.

Steenburgh, W.J., Massey, J.D., and Painter, T.H., 2012, Episodic Dust Events of Utah's Wasatch Front and Adjoining Region: Journal of Applied Meteorology and Climatology, v. 51, p. 1654–1669, doi:10.1175/JAMC-D-12-07.1.

Takemura, T., Uno, I., Nakajima, T., Higurashi, A., and Sano, I., 2002, Modeling study of long-range transport of Asian dust and anthropogenic aerosols from East Asia: Geophysical Research Letters, v. 29, p. 11-1-11–4, doi:10.1029/2002GL016251.

Tokalıoğlu, Ş., and Kartal, Ş., 2006, Multivariate analysis of the data and speciation of heavy metals in street dust samples from the Organized Industrial District in Kayseri (Turkey): Atmospheric Environment, v. 40, p. 2797–2805, doi:10.1016/j.atmosenv.2006.01.019.

von Uexküll, O., Skerfving, S., Doyle, R., and Braungart, M., 2005, Antimony in brake pads-a carcinogenic component? Journal of Cleaner Production, v. 13, p. 19–31, doi:10.1016/j.jclepro.2003.10.008.

VanCuren, R.A., and Cahill, T.A., 2002, Asian aerosols in North America: Frequency and concentration of fine dust: Journal of Geophysical Research: Atmospheres, v. 107, p. AAC 19-1-AAC 19-16, doi:10.1029/2002JD002204.

van Velzen, D., Langenkamp, H., and Herb, G., 1998, Antimony, its sources, applications and flow paths into urban and industrial waste: a review: Waste Management & Research, v. 16, p. 32–40, doi:10.1177/0734242X9801600105.

Wake, C.P., Mayewski, P.A., Li, Z., Han, J., and Qin, D., 1994, Modern eolian dust deposition in central Asia: Tellus B: Chemical and Physical Meteorology, v. 46, p. 220–233, doi:10.3402/tellusb.v46i3.15793.

Washington, R., Todd, M., Middleton, N.J., and Goudie, A.S., 2003, Dust-Storm Source Areas Determined by the Total Ozone Monitoring Spectrometer and Surface Observations: Annals of the Association of American Geographers, v. 93, p. 297–313, doi:10.1111/1467-8306.9302003.

Wen, H., and Carignan, J., 2007, Reviews on atmospheric selenium: Emissions, speciation and fate: Atmospheric Environment, v. 41, p. 7151–7165, doi:10.1016/j.atmosenv.2007.07.035.

Williams, K.T., 1935, Occurence of Selenium in the Colorado River and some of its Tributaries: Industrial & Engineering Chemistry Analytical Edition, v. 7, p. 431–432, doi:10.1021/ac50098a031.

Wong, M.H., Wu, S.C., Deng, W.J., Yu, X.Z., Luo, Q., Leung, A.O.W., Wong, C.S.C., Luksemburg, W.J., and Wong, A.S., 2007, Export of toxic chemicals – A review of the case of uncontrolled electronic-waste recycling: Environmental Pollution, v. 149, p. 131–140, doi:10.1016/j.envpol.2007.01.044.

Wurtsbaugh, W.A., Miller, C., Null, S.E., DeRose, R.J., Wilcock, P., Hahnenberger, M., Howe, F., and Moore, J., 2017, Decline of the world's saline lakes: Nature Geoscience, v. 10, p. 816–821, doi:10.1038/ngeo3052.

Zhang, J., 1994, Atmospheric Wet Deposition of Nutrient Elements: Correlation with Harmful Biological Blooms in Northwest Pacific Coastal Zones: Ambio, v. 23, p. 464–468.

Zhao, W., Sun, Y., Balsam, W., Zeng, L., Lu, H., Otgonbayar, K., and Ji, J., 2015, Clay-sized Hf-Nd-Sr isotopic composition of Mongolian dust as a fingerprint for regional to hemispherical transport: Geophysical Research Letters, v. 42, p. 2015GL064357, doi:10.1002/2015GL064357.